



HAL
open science

Highly Synergistic Properties of Multicomponent Hydrogels Thanks to Cooperative Nucleopeptide Assemblies

Paul Hoschtettler, Guillaume Pickaert, Alain Carvalho, Marie-Christine Averlant-Petit, Loïc Stefan

► **To cite this version:**

Paul Hoschtettler, Guillaume Pickaert, Alain Carvalho, Marie-Christine Averlant-Petit, Loïc Stefan. Highly Synergistic Properties of Multicomponent Hydrogels Thanks to Cooperative Nucleopeptide Assemblies. *Chemistry of Materials*, 2023, 35 (11), pp.4259 - 4275. 10.1021/acs.chemmater.3c00308 . hal-04281977

HAL Id: hal-04281977

<https://hal.univ-lorraine.fr/hal-04281977>

Submitted on 13 Nov 2023

HAL is a multi-disciplinary open access archive for the deposit and dissemination of scientific research documents, whether they are published or not. The documents may come from teaching and research institutions in France or abroad, or from public or private research centers.

L'archive ouverte pluridisciplinaire **HAL**, est destinée au dépôt et à la diffusion de documents scientifiques de niveau recherche, publiés ou non, émanant des établissements d'enseignement et de recherche français ou étrangers, des laboratoires publics ou privés.

1 Highly synergistic properties of multicomponent
2 hydrogels thanks to cooperative nucleopeptide
3 assemblies

4
5 Paul Hoschtettler,^a Guillaume Pickaert,^a Alain Carvalho,^b Marie-Christine Averlant-Petit,^a Loïc
6 Stefan*^a

7 ^a Université de Lorraine, CNRS, LCPM, F-54000 Nancy, France

8 ^b Institut Charles Sadron, UPR 22, Université de Strasbourg, CNRS, 67034 Strasbourg, France

9
10 Corresponding author email: loic.stefan@univ-lorraine.fr

11

12

13 **ABSTRACT**

14 Supramolecular materials have drawn much attention in the past years, particularly because of their
15 great versatility in terms of structures, organization, and types of nano-objects they can form.
16 Among them, amino acid and peptide derivatives are biomolecules extensively used thanks to their
17 inherent properties and applicability for biological and health applications. Their exceptional
18 abilities to self-assemble have been harnessed to create a myriad of objects and materials, including
19 hydrogels. However, the use of one and only one molecule (*i.e.*, monocomponent) is the widely
20 reported approach which offers a great interest in terms of simplicity of use, but numerous
21 limitations in terms of properties. To tackle these issues, the multicomponent approach is a
22 promising strategy, even if challenging for designing low-molecular weight molecules able to
23 interact each other to create new assemblies and new properties not achievable with a single
24 compound. In this context, we report herein on the design, synthesis and multiscale analysis of an
25 original series of nucleopeptides, *i.e.*, comprised both peptide and DNA-nucleobase moieties linked
26 covalently. Thanks to their dual nature, these nucleopeptides are able to coassemble when
27 complementary nucleobase moieties interact intermolecularly via hydrogen bonding and π -
28 stacking interactions, leading to impressive synergistic effects resulting in mechanical properties
29 improved by more than 270.000 % (with stiffness up to > 700 kPa) and self-assembly abilities by
30 ~ 280 %. To decipher the structure/properties relationships, a comprehensive multiscale analysis
31 approach (including rheology, fluorescence, cryoSEM and TEM, FTIR, CD and NMR HR-MAS)
32 has been carried out to understand the impact of nucleobases on the supramolecular assembly
33 process and the subsequent formation of nanoobjects, three-dimensional architectures of the
34 hydrogel scaffold and the resulting physicochemical and mechanical properties of these highly
35 synergistic nucleopeptide assemblies.

36 INTRODUCTION

37 More challenging to design but also much more attractive than mono-component materials, multi-
38 component systems are of growing interest in the field of *soft matter*. Indeed, it has been known
39 for a long time that the use of several chemical constituents is a method of choice to design and
40 synthesize materials with new properties which could not be obtained with one, and only one,
41 chemical. This is especially true for metal polymers and composites,^{1,2} alloys,³ metal-organic
42 frameworks,⁴ or even gels. In the particular case of low-molecular weight peptide-based hydrogels,
43 a type of bioinspired soft materials in the spotlight for more than twenty years,⁵⁻⁸ research and
44 development of multi-component systems are currently attracting the attention of the scientific
45 community due to their promising high potential.⁹⁻¹¹ The use of proteins, peptides, and peptide
46 derivatives to formulate gels and mainly hydrogels, relies both on the intrinsic properties of specific
47 peptide sequences to self-assemble thanks to several intermolecular low energy interactions
48 (including hydrogen bonds, van der Waals and electrostatic forces or π - π and hydrophobic
49 interactions), and on their wide variety in terms of structure (*i.e.*, length of sequence, position and
50 nature (*e.g.*, aromatic, aliphatic, acidic, basic) of the amino acids). Also, their inherent properties
51 of biocompatibility, biodegradability and their generally low immunogenicity^{12,13} have allowed
52 their applications in the biological and biotechnological fields in, for instance, tissue engineering,
53 regenerative medicine, controlled release of bioactive compounds, bioprinting, or as media for cell
54 culture.¹⁴⁻¹⁹ Interestingly, to optimize the properties of mono-component peptide-based hydrogels,
55 the main reported strategies have been the introduction of chemical modifications to the sequence,
56 from aliphatic chains to aromatic moieties, halogenated and non-natural amino acids, among
57 others.^{8,19,20} However, instead of focusing on subtle changes of the gelification-inducing molecule,
58 another approach can be considered to unlock the limitations induced by the use of one, and only

59 one, compound to design next-generation materials: the multi-component-based strategy.⁹⁻¹¹
60 Widely used in Nature and biological systems, the design of such materials is far from trivial, and
61 the choice of the sequence of the peptide derivatives remains highly challenging.^{9,21,22} Recent
62 results have confirmed the high potential and relevance of such an approach, with multicomponent
63 peptide-based hydrogels allowing a precise control of the mechanical properties,²³⁻²⁵ kinetics of
64 formation,^{26,27} or morphologies of the nanostructures,^{28,29} depending on the ratio between the
65 peptide derivatives and/or their nature. Moreover, the multicomponent approach has been reported
66 to bring new properties such as photophysical^{30,31} or electronic³² ones, biofunctionalization³³⁻³⁵ or
67 also further sensitivities to stimuli such as temperature,²⁹ pH³⁶⁻³⁸ or several of them³⁹ (*i.e.*, multi-
68 responsivity). However, applications of multicomponent peptide-based hydrogels are still in their
69 infancy, mainly harnessed in a biological context (*e.g.*, for wound dressing⁴⁰ and dental care⁴¹)
70 thanks to their good biocompatibility.^{23,26,42-44}

71 The formulation of such soft materials remains challenging because, depending on the structure of
72 the peptides, their possible chemical modification(s) and the experimental conditions/mode of
73 preparation, three main types of assemblies can occur,^{10,11} known as: *i-*) self-sorting (*i.e.*, in which
74 each gelator self-assemble with the same gelator)^{36,38,45}; *ii-*) co-assembling (*i.e.*, several gelators
75 interact each other) which can be cooperative (*i.e.*, exhibiting a certain degree of organization) or
76 random,^{24,26,40,46} and *iii-*) disruptive.⁴⁷ However, several main approaches have been proposed in
77 the last decade, with the mix of peptides containing aromatic moieties (*e.g.*, Fmoc),^{23,26,45,48,49}
78 stereoisomers,^{50,51} oppositely charged^{36,37,43,52} or cross-linked^{53,54} peptides, among others.^{11,40,55} In
79 particular, the introduction of DNA-nucleobases in peptide sequences is emerging in the field of
80 supramolecular gels, as recently reviewed.⁵⁶ While most of these nucleopeptide-based hydrogels
81 are mono-component, some examples of multicomponent formulations highlight the benefits of

82 introducing DNA-nucleobases. Indeed, thanks to their inherent ability to self-assemble, mainly *via*
83 H-bonding and π -stacking, to form, *inter alia*, the canonical pairings adenine/thymine (A/T) and
84 guanine/cytosine (G/C), nucleobases are excellent tools to develop complex supramolecular
85 systems with controlled intermolecular interactions.⁵⁷⁻⁵⁹ For instance, the mix of the Adenine-Phe-
86 Phe with Thymine-Phe-Phe leads to an hydrogel with a storage modulus $G' = 18$ kPa, better than
87 each compound alone, while the same approach with the tripeptide Phe-Phe-Tyr has deleterious
88 effects (G' decreasing from 2.1 kPa to 0.2 kPa).⁶⁰ Later, the same group reported on the use of two
89 pentapeptides, namely Leu-Gly-Phe-Asn-Ile and Lys-Thr-Thr-Pro-Val able to co-assemble and
90 form hydrogels when thymine and adenine, respectively, are grafted on the N-term.⁶¹ When only
91 thymine derivatives are mixed, the mechanical properties decrease from $G' = 8.9$ kPa to 0.9 kPa,
92 attesting the importance of the presence of complementary bases. Similar tendencies were also
93 observed with the triphenylalanine peptide for which the multicomponent hydrogels containing the
94 complementary nucleobases (*i.e.*, A/T or G/C) show an improvement of the stiffness, better than
95 with non-complementary (*i.e.*, mismatches) nucleobases and than each compound alone.⁶² The
96 results, correlated with molecular dynamics simulation, suggest the formation of Watson-Crick and
97 π -stacking interactions. Also, our group confirmed that the presence of complementary nucleobases
98 is beneficial for the mechanical and physicochemical properties.⁶³ Other more complex systems
99 were reported by Nilsson⁶⁴ and Stupp⁶⁵ groups in which the addition of external specific single-
100 stranded DNA can modulate the properties of two-component nucleopeptide-based hydrogels.
101 Altogether, although these systems are still under-researched, these data highlight the relevance of
102 using nucleopeptides to develop multi-component peptide-based hydrogels, harnessing both the
103 self-assembly abilities of peptide sequences and the well-known self-organization capability of
104 nucleobases to drive the global assembly process.

105 In this context, we would like to report herein on a new series of co-assembling nucleopeptides
106 based on a short amphipathic peptide sequence on which two different and complementary
107 nucleobase-incorporating moieties (introduced *via* PNA (*for peptide nucleic acid*) strand) were
108 incorporated in order to drive and improve the co-assembly process. To understand and decipher
109 the origin of the high synergistic effects and of the resulting properties of these multicomponent
110 hydrogels, such properties and their relationship with the structure(s), a multi-scale approach has
111 been carried out and is discussed herein.

112

113 **MATERIALS AND METHODS:**

114 **Peptide synthesis, purification and chemical analysis**

115 Peptide derivatives were synthesized both manually and on an automated ResPep XL synthesizer
116 (Intavis AG) using a Fmoc/^tBu strategy and double couplings for each amino acid and PNA moiety.
117 Fmoc-Rink resin (0.64 mmol.g⁻¹, 200-400 mesh) was used and deprotected using piperidine (20%
118 in DMF, 15 min under agitation, twice). The standard experimental conditions for each coupling
119 were: Fmoc-amino acid (5.5 equivalents), 2-(1*H*-benzotriazol-1-yl)-1,1,3,3-tetramethyl-uronium
120 tetrafluoroborate (HBTU, 5 equivalents), and 4-methylmorpholine (NMM, 10 equivalents) in
121 dimethylformamide (DMF) and *N*-methyl-2-pyrrolidone (NMP), coupling time = 40 minutes.
122 Fmoc-PNA-G(Bhoc)-OH, PNA-A(Bhoc)-OH, Fmoc-PNA-C(Bhoc)-OH, Fmoc-PNA-T-OH were
123 introduced manually (3.1 equiv.) using PyBOP (3.0 equiv.), DIPEA (3.0 equiv.) and 2,6-lutidine
124 (4.5 equiv.) in DMF and NMP (double coupling, 2 hours, room temperature, 400 rpm). Acetylation
125 was carried out using a anhydride acetic/2,6-lutidine/DMF (5/6/89) mixture (3 times, 15 min, 400
126 rpm). Fmoc-deprotection steps were carried out using a 20% piperidine solution in DMF (3×15

127 min), and final cleavages were achieved using a trifluoroacetic acid/triisopropylsilane/water
128 (92,5/5/2,5) mixture for 2 hours. The crude peptides were precipitated from cold diethylether (-20
129 °C), centrifuged (3 x 5000 rpm, 5 min), washed with cold diethylether and dried. Then, peptide
130 derivatives were dissolved in solvent A (95 % water, 5 % acetonitrile, 0.1 % trifluoroacetic acid),
131 sonicated, and purified by semi-preparative HPLC equipped with a Nucleosil (Macherey-Nagel)
132 100-5 C₁₈ 250×21 mm column using solvents A and B (100 % acetonitrile, 0.1 % trifluoroacetic
133 acid) with a 5-min isocratic elution (100% solvent A) followed by a linear gradient (from 0 to 100%
134 solvent B, 20 min) 0% to 40 % solvent B) with a UV detection at 214 nm. The resulting solutions
135 were evaporated under reduced-pressure and double-lyophilized.

136 The purity of each peptide was evaluated by analytical reversed-phase HPLC equipped with a
137 Nucleosil (Macherey-Nagel) 100-5 C₁₈ 250×4.6 mm column using solvent A' (95 % water, 5 %
138 acetonitrile, 0.1% formic acid) and solvent B' (100 % acetonitrile, 0.1 % formic acid) with a 5-min
139 isocratic elution (100 % A') followed by a 10-min linear gradient (0 % to 100 % solvent B') and a
140 5-min linear gradient (60 % to 100 % B') with a UV detection at 214 nm. High resolution ESI-MS
141 analyses were performed on a Bruker Daltonics MicroTOFQ mass spectrometer (MassLor
142 platform, Univ. Lorraine) and all the compounds were fully characterized by NMR ¹H, COSY,
143 TOCSY, NOESY, ROESY, ¹³C-¹H HSQC NMR experiments in a Bruker Advance NEO 400 MHz
144 instrument equipped with a BBFO smart probe in DMSO ([sample] = 10 mM). Data were acquired
145 and transformed using Bruker Topspin 4.1.1 software assignment was done using
146 NMRFAM_spark software.⁶⁶

147 **Sample preparation**

148 As a global procedure, the samples were prepared at a total concentration of 15 mM dissolving
149 each sample in Tris.HCl (1 M, pH 7.4). All the buffers were prepared in deionized water (18.2

150 M Ω .cm) or D₂O (for FTIR experiments). As a standard procedure, the glass vials containing the
151 solutions were sealed and subsequently heated (heatgun with a variable temperature control, 70 °C,
152 3 min), to ensure a complete dissolution of the starting powders. Samples were used directly
153 (rheology, Thioflavin T and Thiazole orange fluorescence experiments) or stored 24 hours at room
154 temperature before analysis.

155 **Rheological characterizations**

156 Dynamic rheological measurements were performed on an AR2000 rheometer (TA Instruments)
157 operating in oscillatory mode, equipped with a Peltier plate temperature control and a Couette
158 geometry immersed inside the samples, as already described.⁶⁷ All the measurements were
159 performed on 300- μ L samples and repeated a minimum of three times and 20°C. Frequency sweep
160 experiments were conducted at constant applied stress (1 Pa) for a range of 0.1-100 rad.s⁻¹. Stress
161 sweep experiments were performed for a range of 0.46-1000 Pa applied stress at a 1 rad.s⁻¹ angular
162 frequency. The limiting values of the linear viscoelastic region (*i.e.*, the yield point τ_y) correspond
163 to the stress value at which the storage modulus loses 10% of its maximal value). For thixotropy
164 experiments, the samples underwent consecutive rest (constant applied stress (1 Pa)) and break
165 (100% strain amplitude) steps. The storage (G') and loss (G'') moduli reported were chosen at the
166 end of each step.

167 **Electron microscopy**

168 For cryo-scanning microscopy (cryo-SEM), a piece of hydrogel was placed on a home-made cryo-
169 holder and quickly plunged into an ethane slush. The sample was rapidly frozen during the plunging
170 by direct contact with the liquid ethane in order to form amorphous ice. Subsequently, the sample
171 was transferred into the Quorum PT 3010 chamber attached to the microscope. There, the frozen

172 sample was fractured with a razor blade. A slight etching at -90°C may be performed to render the
173 sample more visible. The sample is eventually transferred in the FEG-cryoSEM (Hitachi SU8010)
174 and observed at 1 kV at -150°C . Several sublimation cycles were performed on each sample to
175 ensure the removal of the ice from the hydrogel. A FFT bandpass filter may be used with FiJi
176 software to suppress horizontal stripes that were created by scanning the image line by line.

177 Transmittance Electron Microscopy (TEM) experiments were performed on a Philips CM200
178 electron microscope operating at 200 kV and fitted with CCD MSC 600 Gatan camera (Institut
179 Jean Lamour, Université de Lorraine/CNRS, Nancy, France). Samples were prepared by placing a
180 drop of each sample (15 mM) on 200-mesh carbon-coated copper grids (CF-200-Cu-50) for 1 min.
181 The excess fluid was subsequently removed and a drop of phosphotungstic contrasting agent (2%
182 w/w in deionized water) was deposited for 0.5 min. The excess was subsequently removed and the
183 grid was air-dried for 10 min before analysis. Collected data were analyzed using Gatan
184 DigitalMicrograph and FiJi software.

185 **FTIR**

186 For FTIR experiments, samples were prepared as above-mentioned in a solution of Tris.HCl (pH
187 7.4) prepared in D_2O in order to suppress the strong water absorbance in the $1600\text{-}1700\text{ cm}^{-1}$
188 spectral region (corresponding to the amide I and nucleobase vibration region).^{68,69} *Nota: additional*
189 *TEM and FTIR assays were carried out to confirm that D_2O do not impact the supramolecular*
190 *assemblies and the nanostructures formed (see Supporting Information).* FTIR measurements were
191 carried out at room temperature on a Invenio S spectrometer (Bruker) equipped with an ATR
192 Specac diamond (Quest), in a range of $4000\text{-}400\text{ cm}^{-1}$ with a 2 cm^{-1} -resolution. Infrared spectra
193 represent an average of 128 scans recorded in a single-beam mode and corrected for the

194 background. Data were analyzed, smoothed (Savitzky-Golay, 2nd order, 13 points), and treated
195 using the OPUS software.

196

197 **Circular dichroism**

198 Circular dichroism spectra were recorded using a Chirascan Plus spectrophotometer (Applied
199 Photophysics, UMS 2008 IBSLor platform, Université de Lorraine/CNRS/INSERM, Nancy,
200 France) at 20°C. Hydrogels were prepared in an aqueous solution of NaF (500 mM in deionized
201 water (18.2 MΩ.cm) adjusted to pH = 7.4 with NaOH) at a final concentration of peptide of 10
202 mM. The samples were deposited carefully inside a 0.01-cm-pathlength dismountable cuvette prior
203 to be analyzed. Their spectra were measured between 180-320 nm (step = 0.5 nm, response = 0.5
204 s, bandwidth = 1 nm) averaged on three repetitions. After background subtraction and smoothing
205 (Savitzky-Golay, 2nd order, 13 points), all raw data (θ , mdeg) were converted into mean residual
206 ellipticity (MRE) according to the equation below:

$$207 \quad \text{MRE} = \frac{\theta}{(n - 1) \times c \times d \times 10}$$

208 where MRE is in deg.cm².dmol⁻¹, d is the cuvette pathlength in cm, and c the molar concentration
209 in mol·L⁻¹.

210 **Fluorescence**

211 Fluorescence spectra were recorded using a FP-8300 spectrofluorometer (JASCO Corp.) on 7.5
212 mM samples in Tris.HCl buffer (1 M, pH 7.4). For each experiment 800 μ L of the samples were
213 transferred into quartz cuvettes (1 x 0.3 cm-pathlength). Fluorescence spectra were obtained at 20
214 °C with a 3D measurements mode (parameters: scanning speed = 200 nm/min, response time = 1

215 sec, emission bandwidth = 5 nm and excitation bandwidth = 1 nm). Excitation spectra were
216 recorded from 290 to 420 nm (step = 1 nm) for an emission wavelength varying from 302 to 580
217 nm (step = 2 nm), and emission spectra were recorded from 300 nm to 600 nm (step = 1 nm) for
218 an excitation wavelength varying from 290 to 420 nm (step = 2 nm). Data were processed and
219 smoothed (Savitzky-Golay, 2nd order, 9 points) using OriginPro 8.5. For the determination of the
220 REES phenomenon, the maximum of emission is spotted on each smoothed emission spectrum for
221 all compounds as a function of the excitation wavelength. Subsequently, the graph $\lambda_{em} = f(\lambda_{ex})$ was
222 plotted and fitted by a linear regression.

223 **Thioflavin T and Thiazole orange fluorescence experiments.**

224 Fluorescence spectra were recorded on a Varioskan LUX microplate reader (Thermo Fisher) at
225 20°C using black 96-well microplates. Stock solutions of Thioflavin T (ThT, 750 μ M) and Thiazole
226 orange (TO, 200 μ M) were prepared in deionized water (18.2 M Ω .cm), and the actual
227 concentrations were determined through UV-vis spectral analysis at 412 nm ($\epsilon_{412nm} = 36000 \text{ M}^{-1}$
228 $\cdot\text{cm}^{-1}$)⁷⁰ and 500 nm ($\epsilon_{500nm} = 63000 \text{ M}^{-1}\cdot\text{cm}^{-1}$)⁷¹, respectively. Samples were prepared mixing the
229 ThT or TO solution with peptide derivative solutions (previously dissolved in Tris.HCl (1 M, pH
230 7.4)) to reach final concentrations of [ThT] = [TO] = 50 μ M and of each peptide derivative from
231 2.5 to 15 mM. Samples were subsequently transferred into microplates (150 μ L per well), protected
232 with an optical adhesive film (to avoid evaporation) and the fluorescence was measured during 24
233 hours using the following parameters: measurement time = 1 sec, excitation bandwidth = 12 nm,
234 automatic dynamic range, kinetic interval = 2 min, continuous shaking time between readings (60
235 rpm, low force), 20°C, with $\lambda_{ex} = 440 \text{ nm}$, $\lambda_{em} = 485 \text{ nm}$ for ThT, $\lambda_{ex} = 500 \text{ nm}$, $\lambda_{em} = 540 \text{ nm}$ for
236 TO. Fluorescence emissions were plotted as a function of time, and results are mean of four
237 experiments. Characteristic values were extracted from the graphs: the inflexion point

238 corresponding to the time at which the 1st derivative is at its maximum, the apparent growth rate
239 k_{app} calculated from the tangent at the inflexion point, and the lag time t_{lag} corresponds to the
240 intercept between the above-mentioned tangent and the baseline.⁷²

241 **NMR experiments (HR-MAS)**

242 Gels were prepared at a total concentration of 15 mM of the nucleopeptides mix in a solution of
243 TrisHCl-d₁₁ (1M pH = 7.4) with 5% D₂O. After being shaken at 70°C for 3 min the sample were
244 transferred in a 4 mm ZrO₂ MAS rotor, experiments were run after 24 hours. The 1D experiments
245 were acquired with a rotation speed of 4000 Hz on a Bruker Advance NEO 400 MHz NMR
246 spectrometer equipped with a 4mm HR-MAS probe. Water suppression was done using watergate
247 sequence.⁷³

248

249 **RESULTS AND DISCUSSION**

250 **Design and synthesis of a new series of nucleopeptide-based hydrogelators**

251 In the development of nucleopeptide-based hydrogels, our group have already reported a series of
252 amphipathic peptides Glu-Phe-Glu-(Phe-Lys)₂ functionalized at its *N*-term by a PNA moiety
253 incorporating one of the four DNA nucleobase (*i.e.*, adenine (A), thymine (T), guanine (G) and
254 cytosine (C)). Used alone to formulate hydrogels,⁶⁷ we demonstrated that depending on the nature
255 of the nucleobase, the mechanical and physicochemical properties can be drastically improved and
256 finely tuned, thanks to subtle structural modulations from the (supra)molecular to the microscopic
257 scale (*e.g.*, intermolecular interactions *via* twisted β -sheets, size and morphology of the fibrillar
258 network). Mixing these compounds to develop more complex multicomponent systems showed
259 that hydrogels properties are heightened in the presence of two nucleopeptides bearing

260 complementary nucleobases,⁶³ even if they do not exhibit significant synergistic effects. We
261 subsequently hypothesized that the nucleobase/amino acid ratio of 1/7 was too low, leading to co-
262 assembly processes mainly driven by the peptide part and in which the nucleobases only bring fine
263 modulations of the structural organization, limiting the high potential of such systems. Thus, we
264 report herein on a series for nucleopeptides build from the short amphipathic tetrapeptide Phe-Glu-
265 Phe-Lys (*i.e.*, FEFK)⁷⁴ on which PNA strands of two units were incorporated at the N-term,
266 improving the nucleobase/amino acid ratio to 1/2 to favor the impact and recognition of
267 nucleobases. Herein, PNA (for peptide nucleic acids) derivatives, already considered for the
268 development of nucleopeptides by our group^{63,67} and others,^{56,75} were chosen thanks to their high
269 chemical stability, the more stable pairing they form, their simplicity of chemical synthesis (and of
270 scalability), and their relevance in material science and for biological applications.^{76,77} Thus, two
271 PNA sequences were selected, each containing one purine and one non-complementary pyrimidine,
272 namely adenine-cytosine (AC) and thymine-guanine (TG) (**Fig. 1A**), which are complementary
273 sequences but not self-complementary in order to avoid homomolecular interactions and favor
274 heteromolecular ones, a *sine qua non* conditions to reach synergistic effects and innovative
275 properties, thanks to peptide/peptide and nucleobase/nucleobase interactions, as proposed **Fig. 1B**.
276 Hence, a series of five compounds (**Fig. 1A**), both amidated and acetylated at their C- and N-term,
277 respectively, were synthesized on solid support at a 800 μ mol-scale: **p(TG)-FEFK** and **p(AC)-**
278 **FEFK**, and also the two controls **p(CC)-FEFK** and **p(TT)-FEFK** (for which the design will be
279 discussed *vide infra*), and the nucleobase-lacking native peptide FEFK. All the (nucleo)peptides
280 were obtained with yields up to 77%, purified by reverse-phase HPLC (purity \geq 98.9%), and fully
281 characterized by LC-MS, ESI-HRMS, ¹H, ¹³C and 2D NMR (COSY, NOESY, TOCSY and
282 ROESY in DMSO-*d*₆). Detailed protocol and characterizations are available in the Material and
283 methods section and in the ESI, respectively.

284

285 **Synergistic effect of nucleopeptide mixtures on the mechanical properties**

286 To evaluate the abilities of the compounds to form hydrogels, we first used the tube inversion test
287 in physiological conditions using buffer Tris.HCl (pH 7.4) only, without the presence of co-solvent
288 such as the often-used DMSO. Using these conditions, we first observed (**Fig S1**) that **p(AC)-**
289 **FEFK** fails to form a gel and stays liquid even after a month up to a concentration of 60 mM, while
290 **p(TG)-FEFK** is able to gelify as a transparent and weak hydrogel at a minimum concentration of
291 12 mM (requiring more than 2 days). By contrast, the formulation of their equimolar mixture leads
292 to a strong transparent and homogeneous gel after 120 min at 15mM (critical gelification
293 concentration (or CCG) = 8 mM, 4 days) showing a synergistic effect between the two
294 nucleopeptides. Based on these preliminary data and on previous work^{78,79} including our,^{63,67} we
295 selected 15 mM as the standard concentration for the following studies. To assess quantitative
296 values, we then performed a series of rheological investigations (frequency and stress sweep
297 experiments), in triplicates, with 24h-aged hydrogels (Tris.HCl buffer, pH 7.4). In accordance with
298 the visual observations, the storage moduli of the compounds alone are < 10 Pa and 1.3kPa for
299 **p(AC)-FEFK** and **p(TG)-FEFK**, respectively (**Fig. 2A,B, Fig. S2**). Mixing these two compounds
300 leads to drastic improvements of the mechanical properties, with the stiffest hydrogel obtained for
301 the equimolar ratio with $G' = 61,7$ kPa, while the 3/1 and 1/3 (in purple and brown red, respectively,
302 **Fig. 2A,B, Fig. S2**) **p(AC)-FEFK/p(TG)-FEFK** molar ratios lead to hydrogels with $G' = 11.9$ kPa
303 and 22.5 kPa, respectively. The experiments clearly highlight the synergistic effect of the
304 multicomponent hydrogel formulations, which is also confirmed by the evaluation of their
305 resistance to stress, characterized by the yield point τ_y obtained at the limiting value of the linear
306 viscoelastic region (*i.e.*, corresponding to the maximum stress that can be imposed to the gel before

307 destroying it). Indeed, τ_y is < 1 Pa and 1.3 Pa for p(AC)-FEFK and p(TG)-FEFK alone,
308 respectively (**Fig. 2C,D, Fig. S4**), while mixing them at 3/1 and 1/3 ratio significantly improves
309 these values to $\tau_y = 14.3$ and 7.8 Pa, respectively. The highest resistance to stress is obtained in
310 equimolar conditions (in red, **Fig. 2C,D**) with $\tau_y = 86$ Pa, *i.e.*, more than 67 times better than the
311 compounds alone.

312 To evaluate and decipher the roles and impacts of the peptide nucleic acid sequence on these
313 mechanical synergistic effects, we considered and synthesized three other (nucleo)peptide
314 derivatives (**Fig. 1A**): *i-*) p(CC)-FEFK which bears in its PNA sequence one complementary
315 nucleobase and one mismatch with p(TG)-FEFK (*i.e.*, cytosine-guanine and cytosine-thymine,
316 respectively), *ii-*) p(TT)-FEFK which have two mismatches in its PNA sequence with p(TG)-FEFK
317 (*i.e.*, thymine-guanine and thymine-thymine), *iii-*) the PNA-lacking sequence FEFK. Thus, we first
318 measured the rheological properties of these compounds alone (at 15mM, buffer Tris.HCl pH 7.4,
319 **Fig. S3** and, secondly, mixed with TG-FEFK in an equimolar ratio and at the same total molar
320 concentration (*i.e.*, 15 mM, in buffer Tris.HCl, pH 7.4). The data reported **Fig. 3A-C** (and **Fig. S6**)
321 highlight that the greatest improvement is obtained when the two nucleopeptides bearing the two
322 complementary nucleobase-sequences, *i.e.*, p(TG)-FEFK + p(AC)-FEFK are mixed together,
323 with %improvement $> 270\ 000\%$ (in red, **Fig. 3B** and **Fig. S6**). Then, the presence of one mismatch
324 in the PNA sequence of p(CC)-FEFK significantly decreases this synergistic effect by a factor of
325 ≈ 135 (%improvement $\approx 2\ 000\%$, in green, **Fig. 3B** and **Fig S6**) which is even lower when there are
326 two mismatches in the PNA sequence, *i.e.*, with p(TT)-FEFK (%improvement $\approx 480\%$, in dark
327 cyan **Fig. 3B** and **Fig. S6**). These results support that the synergistic effect relies on supramolecular
328 co-assemblies which are dependent on the complementarity of the PNA-nucleobase sequences.
329 Moreover, the use of the PNA-lacking FEFK tetrapeptide results in %improvement (181%, in

330 orange **Fig. 3B** and **Fig. S6** close to the non-complementary **p(TT)-FEFK**, confirming the role of
331 complementary nucleobases on the co-assembly processes and the subsequent synergistic effects
332 which are the highest for the equimolar mixture of **p(AC)-FEFK** and **p(TG)-FEFK**. Remarkably,
333 this latter mixture allows the formation of stable, homogeneous and of the stiffest hydrogel (among
334 all the studied samples) with a storage modulus > 60 kPa at 15 mM (**Fig. 2A,B**), which is highly
335 competitive compared to other low-molecular weight peptide-based hydrogels at the same
336 concentration (*e.g.*, ≈ 18 kPa for Ac-ILVAGK-NH₂,⁸⁰ ≈ 20 kPa for DF(I)NKF(I),⁷⁸ ≈ 40 kPa for
337 PNA(G)-EFE(FK)₂,⁶⁷ ≈ 90 kPa for Thy-KFF⁶²). Also, increasing the total concentration of this
338 equimolar mixture leads to a maximum $G' = 720$ kPa obtained at 60 mM (**Fig. S7**), making this
339 hydrogel one of the stiffest peptide-based hydrogels reported so far (*e.g.*, ≈ 190 kPa for the
340 equimolar mixture Fmoc-FF and Fmoc-F(F₅),⁴⁹ < 300 kPa for HO-YL-Suc-FY-OH,⁸¹ ≈ 310 kPa for
341 (FQ)₂-F(I)K-NH₂,⁸² ≈ 1000 kPa for cyclo[FC]⁸³). Interestingly, the 1/1 **p(AC)-FEFK/p(TG)-**
342 **FEFK** hydrogel exhibits excellent thixotropic properties (also termed self-healing), meaning that
343 under high stress beyond the yield point τ_y , the hydrogel is broken (gel-to-sol transition) but is able
344 to recover its gel properties when the applied stress is decreased below the yield point τ_y . Such
345 properties are of primary importance for biomedical and biotechnological applications such as for
346 drug controlled release, gel dressing or tissue engineering.⁸⁴⁻⁸⁷ In our case, our hydrogel can be
347 loaded into a syringe (**Fig. 3D**) and then squirted through the needle into a vial in which the
348 viscoelastic liquid recovers its gel state after *c.a.* 20 min. Using the rheometer to evaluate these
349 thixotropic properties, we did not observe any significant modifications of the mechanical
350 properties (*see Fig. S8*) even after 9 cycles of breaking/recovery (**Fig. 3E** and **Fig. S9**), confirming
351 the excellent self-healing properties of this hydrogel.

352 **Studies of the hydrogels' scaffolds and morphologies using electron microscopies.**

353 The disparity in terms of mechanical properties observed for the (nucleo)peptides mixtures
354 originates from differences in their mode of assembly and in the tridimensional architectures they
355 form. Thus, both cryo-SEM and TEM, two techniques of choice to study the hydrogel scaffolds,⁸⁸
356 have been used. As observed **Fig. 4** (and **Fig. S10,S14**), **p(AC)-FEFK** alone shows amorphous
357 structures with the presence of few random two-dimensional aggregates, whereas **p(TG)-FEFK**
358 alone exhibits dense entangled networks characterized by ribbon-like structures (13.9 ± 3.1 nm-
359 cross-section, > 200 nm long) and their bundles, already reported for nucleopeptide⁶³ and peptide-
360 based hydrogels, and the presence of small pores (heterogeneous, *circa* 30-50 nm). Mixing these
361 two compounds, which leads to highly synergistic improvements of the mechanical properties (*vide*
362 *supra*), results in a three-dimensional morphology distinct from the compounds alone. Indeed, as
363 observed (**Fig. 4**, right panel and **Fig. S11,S14**), a highly porous morphology is obtained with
364 numerous alveoli (ovoid, *circa* 400-600 nm x 900-1200 nm) that are lined by visible fibres,
365 confirmed by TEM, and with characteristic diameter and length of 6.80 ± 0.68 nm-diameter and
366 up to > 2 μ m, respectively. Such a supramolecular architecture points out that the two
367 complementary nucleopeptides co-assemble *via* specific interactions to form a new peculiar
368 hydrogel scaffold more prone to entrap the solvent (*i.e.*, water molecules) thanks to specific inter-
369 fibrillar interactions and entanglements, as proposed in our design (see **Fig. 1**) and discussed further
370 hereinafter. Interestingly, the two other nucleopeptide mixtures also exhibit porous structures
371 bigger for **p(CC)-FEFK + p(TG)-FEFK** (up to $> 2\mu$ m, **Fig. S13**) which have weaker mechanical
372 properties ($G' \sim 130$ Pa, **Fig. 2**) compared to **p(TT)-FEFK + p(TG)-FEFK** with pores of *circa*
373 300-500 nm x 800-1000 nm and intermediate mechanical properties (*vide supra*). While
374 heterogenous fibrillar and aggregated structures have been observed for the former (**Fig. S16**), the
375 latter assemble into a fibrillar network (17.6 ± 3.1 nm-cross-section, **Fig. S12,S15**). However, the

376 presence of **FEFK** with **p(TG)-FEFK** leads to ill-defined spherical aggregates (**Fig. S11,S17**)
377 leading to the inability of this mixture to form self-supporting hydrogels.

378 **Investigating the supramolecular assemblies at the mesoscopic scales**

379 **To monitor the formation of the** fibrillar networks, observed in electron microscopy, **leading to the**
380 **gelification process**, we considered fluorescence experiments using the well-known Thioflavin T
381 (ThT) “off/on” probe (*i.e.*, while ThT is non fluorescent in solution, **its binding turns on** its
382 fluorescence ($\lambda_{\text{ex}} = 450 \text{ nm}$, $\lambda_{\text{em}} = 485 \text{ nm}$)).^{70,89} Indeed, ThT is widely used in biomedical research,
383 especially in the context of neurodegenerative diseases (*e.g.*, Parkinson’s, Alzheimer’s and Prion’s
384 diseases) in which **proteins or peptides self-assemble into β -sheets fibrils to form *in fine* amyloid**
385 **fibers, but due to its chemical structure, ThT is also a fluorescent molecular rotor sensitive to its**
386 **environment.**^{90,91} Few examples have been reported on the use of this probe in the context of
387 **peptide-based soft matter, which has however been harnessed to assess the abilities of peptide-**^{92,93}
388 **and nucleopeptide-based**^{63,67} hydrogels to form β -sheet assemblies and fibrillar networks, or to
389 **monitor the evolution of their complex viscosity during the gelification process.**⁹⁴ In our case, we
390 first confirmed that the equimolar mixture **p(AC)-FEFK/p(TG)-FEFK** at 15 mM (*i.e.*, same
391 conditions than samples studied in rheology) is responsive to ThT, turning on its fluorescence and
392 consequently supporting the abilities of the two nucleopeptides to co-assemble *via* the formation
393 of β -sheets (**as confirmed by CD and FTIR, *vide infra***). Thus, the evolution of the ThT fluorescence
394 as a function of time, displayed **Fig. 5A,B** shows that the maximum intensity after 24h is reached
395 for the equimolar **p(AC)-FEFK/p(TG)-FEFK** mixture with $I_{\text{max}} \approx 175$, while **p(TG)-FEFK** alone
396 has a lower $I_{\text{max}} \approx 125$ far better than **p(AC)-FEFK** alone which is close to $I_{\text{max}} \approx 3$. Also, for the
397 PNA-lacking **FEFK** tetrapeptide, no signal is detected at 10 mM, and 50 mM are required to
398 measure an intensity ≈ 10 after one day, showing well the low propensity of the tetrapeptide to self-

399 assemble, as already reported.⁷⁴ These data are in perfect accordance with our previous results: on
400 the one hand, **p(AC)-FEFK** is not able to form gels (even at high concentrations) and no specific
401 nano- or micro-structures have been observed by electron microscopy (see *vide supra*) due to its
402 inability to self-assemble, as confirmed by its low ThT fluorescence. On the other hand, **p(TG)-**
403 **FEFK** alone is able to form a gel (even if weak, **Fig. 2A**) due to a fibrillar network revealed by
404 microscopy which is therefore comprised of β -sheet assemblies. Mixing these two nucleopeptides
405 leads to a significant enhancement of the fluorescence intensity, supporting both a synergistic effect
406 and a mode of co-assembly through β -sheet interactions (as confirmed by CD and FTIR, *vide infra*),
407 consistent with the nano-architectures and the high stiffness of the hydrogel they form (*vide supra*).
408 Interestingly, looking at the evolution of ThT fluorescence kinetics points out that for **p(TG)-**
409 **FEFK** alone, the increase of the signal starts immediately after its formulation (*i.e.*, without a lag
410 time) and with an apparent rate constant $k_{app} = 54.6 \text{ h}^{-1}$ to reach a plateau after 280 min. By contrast,
411 the equimolar mixture **p(AC)-FEFK/p(TG)-FEFK** experienced a lag time (*i.e.*, corresponding to
412 the non-fluorescent initial state in which monomers undergo primary nucleations)⁷² of $t_{lag} = 78 \text{ min}$
413 which can be explained by the presence of two nucleopeptides that require a longer time to
414 efficiency nucleate and subsequently form effective early-stage fibrils (indeed, the presence of two
415 components statistically increases the number of intermolecular metastable species that can be
416 formed) before entering into the growth phase.⁷² Plotting the evolution of the lag time and of the
417 inflexion point ($t_{1/2}$) as a function of the total concentration of the equimolar mixture **p(AC)-**
418 **FEFK/p(TG)-FEFK** (in log/log scale, see **Fig. S19**) show linear correlations with scaling
419 exponents $\gamma_{lag} = -1.66$ ($r^2 = 0.987$) and $\gamma_{inf} = -1.76$ ($r^2 = 0.980$). These relevant values, ≤ -1 , are
420 indicative of the main underlying aggregation mechanisms that take place *via* a monomer-
421 dependent secondary-nucleation-dominated mechanism.⁹⁵⁻⁹⁷ Also, comparing the ThT
422 fluorescence kinetic curve with the time sweep rheological experiments at the same concentration

423 (*i.e.*, 15 mM) for the equimolar mixture **p(AC)-FEFK/p(TG)-FEFK (Fig. S20)** clearly highlights
424 that **a first assembly process including** the initial (*i.e.*, the lag time **in which primary nucleations**
425 **occur**) and the growth phase step ($t \sim 150$ min), **corresponding to the formation and growth of**
426 **fibers, respectively, is the *sine qua non* condition to trigger the sol-to-gel transition (monitored by**
427 **rheology) step in which the fibrillar network becomes denser, increasing the mechanical properties**
428 **of the hydrogel.** It should also be noted that for concentration > 5 mM, two transitions are observed
429 in the ThT kinetic graphs: a biphasic curve can indicate either distinctive aggregation processes
430 taking place at different time scales,^{96,98} or the formation of transient and metastable oligomers
431 which then evolve into thermodynamically more stable architectures,^{99,100} **which are two**
432 **hypotheses in accordance with the formation and growth of fibrils followed by the formation of a**
433 **tridimensional network, as discussed hereinbefore.** In any case, these data highlight the complexity
434 of the mechanism of assembly due to the presence of two nucleopeptides bearing complementary
435 nucleobase-containing sequences. Such studies are challenging and far from the scope of this article
436 and will be considered elsewhere; herein, we decided to work with 24h-aged samples in which a
437 thermodynamic equilibrium is reached (in accordance with rheological studies). In order to
438 evaluate and decipher the synergistic effects and the causal relationship with the PNA sequences,
439 as done in rheology (*vide supra*), we compared the impact of the addition of **p(TG)-FEFK** with
440 the aforementioned series of nucleopeptides on the improvement of the ThT fluorescence intensity
441 I_{\max} . In line with the results obtained in rheology, data **Fig 5B,C** (and **Fig. S22**) clearly highlight
442 that the greatest improvement is obtained for the mixture **p(TG)-FEFK/p(AC)-FEFK** (in red, **Fig.**
443 **5B)** with a %improvement of 280%, far better than for the mixtures prepared with **p(TG)-FEFK**
444 in the presence of **p(CC)-FEFK** (bearing one mismatch and one complementary nucleobase) and
445 of **p(TT)-FEFK** (bearing two mismatches) for which %improvement is null. The absence of
446 synergistic effect for the two latter multicomponent samples are indicative of a non-collaborative

447 assembly process between the two non-fully complementary nucleopeptides; even though these
448 results suggest an assembly process *via* self-sorting,¹⁰¹ additional spectroscopic experiments (*e.g.*,
449 CD, FTIR) and microscopy do not support this hypothesis (discussed hereinafter). Altogether, these
450 experiments using the ThT fluorescent probe able to follow the assembly process of amyloid-like
451 structures confirm both the nature of the interactions between nucleopeptides *via* the formation of
452 β -sheets, and the high synergistic effect when two nucleopeptides bearing complementary
453 nucleobase-sequences are brought together.

454 To supplement the fluorescent experiments, another “on/off” probe was selected to monitor the
455 self-assembly of the nucleobases, namely the asymmetric cyanine dye Thiazole Orange (TO).
456 While ThT is specific to peptide (or proteins) aggregations, TO is also non emissive when free in
457 solution and its intense fluorescence is triggered upon binding to double-stranded RNA and DNA
458 oligonucleotides, by intercalating between nucleobase pairs or by binding grooves.^{71,102} Thus,
459 using the same methodology than for ThT, the evolution of the fluorescence was recorded ($\lambda_{\text{ex}} =$
460 500 nm, $\lambda_{\text{em}} = 540$ nm) as a function of time. The same trends have been observed (**Fig. 6A**) with,
461 for instance, a sharp increase for **p(TG)-FEFK** ($k_{\text{app}} = 95.6 \text{ h}^{-1}$) without lag time, while the
462 equimolar mixture **p(TG)-FEFK/p(AC)-FEFK** shows a lag time ($t_{\text{lag}} = 36$ min, shorter than with
463 ThT ($t_{\text{lag}} = 78$ min, which can let us hypothesized that nucleobase intermolecular assemblies
464 precede peptide assemblies), a slower apparent rate constant $k_{\text{app}} = 3.8 \text{ h}^{-1}$, and also the maximum
465 fluorescence intensity with $I_{\text{max}} = 106$ (versus 66 for **p(TG)-FEFK** alone). It is worth noting that
466 the PNA-lacking **FEFK** peptide, while responsive to ThT do not exhibit any signal even at high
467 concentration (50mM), confirming that TO is selective towards nucleobase assemblies and do not
468 interact with the peptide parts. Using the same methodology than for ThT, the synergistic effects
469 of the multicomponent mixtures were evaluated thanks to the %improvement of the fluorescence

470 upon the addition of **p(TG)-FEFK** nucleopeptide to the aforementioned peptide and
471 nucleopeptides. As reported **Fig. 6B,C (and Fig. S24)**, once more, the maximum synergistic effect
472 is obtained for the **p(TG)-FEFK/p(AC)-FEFK** mixture with %improvement of 247% which drops
473 dramatically to 52% and 67% for the two other nucleopeptide multicomponent samples containing
474 **p(CC)-FEFK** and **p(TT)-FEFK**, respectively, in the presence of **p(TG)-FEFK**. These results
475 confirm both the synergistic character of the association of **p(TG)-FEFK/p(AC)-FEFK** and the
476 abilities of the nucleobases to self-assemble, thanks to the light up fluorescence of TO.

477
478 **Deciphering the supramolecular architectures nucleopeptide assemblies form via**
479 **spectroscopic investigations.**

480 Parallel spectroscopic experiments were carried out using circular dichroism (CD) and Fourier-
481 transform infrared (FTIR), two methods of choice to assess structural information about the
482 nucleopeptide assemblies. Thus, we highlight that **p(TG)-FEFK** alone self-assemble *via* the
483 formation of β -sheets, as evidenced by the amide I band centered at 1623 cm^{-1} (FTIR, **Fig. 7A**)¹⁰³
484 and characteristic positive (197 nm) and negative (214 nm) Cotton effects in its CD spectrum (**Fig.**
485 **7B**),¹⁰⁴ while the **p(AC)-FEFK** alone do not self-assemble, with typical random signatures in CD
486 and FTIR (**Fig. 7A,B**). Mixing these two nucleopeptides leads to the formation of an hydrogel with
487 synergistic effects including high stiffness, and with a fibrillar morphology (see microscopy and
488 ThT experiment, *vide supra*) thanks to a supramolecular organization based on antiparallel β -sheet
489 formation, as confirmed by the presence of, *inter alia*, a band at 1620 cm^{-1} in FTIR (in red, **Fig.**
490 **7A**), and both positive and negatives bands in CD at 186 nm (π - π^* transition of the amides) and
491 215 nm (n - π^* transition of the amide), respectively (in red, **Fig. 7B**). Interestingly, the comparison
492 of both the FTIR and CD spectra of the mixture with the arithmetic mean of each constituting
493 nucleopeptide (in yellow, **Fig. 7A,B**) highlight a different signature, discarding a self-sorted

494 assembly and, consequently, supporting a co-assembly process¹⁰¹ between these two components
495 bearing complementary nucleobases, as proposed in our design (**Fig. 1B**) and in accordance with
496 results discussed hereinbefore. Additional FTIR and CD experiments with the other mixtures
497 confirm the inability of **p(CC)-FEFK + p(TG)-FEFK** to interact efficiently (**Fig. 7C,D** and **Fig**
498 **S28,S30**), implying that **p(CC)-FEFK** has a deleterious effect on the supramolecular assembly of
499 **p(TG)-FEFK**, also termed disruptive assembly.^{11,47} However, the simultaneous presence of
500 **p(TT)-FEFK** with **p(TG)-FEFK** forms β -sheet structures as evidenced by CD (positive and
501 negative bands at 197 and 214 nm, respectively, **Fig. 7D**) and FTIR (amide I band at 1622 cm⁻¹,
502 **Fig. 7C**), leading to fibrillar morphologies observed by microscopy (*vide supra*). Surprisingly, the
503 sample FEFK + p(TG)-FEFK, while unable to form self-supporting hydrogels, show typical β -
504 sheet signatures (**Fig 7C,D**), even if no (high)ordered structures are observed in microscopy (*vide*
505 *supra*), which let us suppose the formation of supramolecular assemblies which are unable to grow
506 into organized nano/micro objects.

507 Moreover, for all the samples containing one or two nucleopeptides, we can observe in CD
508 additional bands above 250 nm, which are due to nucleobase chromophores in interaction,^{105,106}
509 confirming the role of the latter on the assembly process. In particular, the most intense band in
510 this region is obtained for **p(AC)-FEFK + p(TG)-FEFK** (**Fig. S31**) which is also the only one
511 negative and which differ the most from the arithmetic mean and of its two constitutive compounds,
512 suggesting a greater involvement of the nucleobases in this specific mixture.

513 Trying to go further into the understanding of the role of the nucleobases in the supramolecular
514 assembly, we carried out fluorescence spectroscopies on all the four mixtures. As displayed **Fig.**
515 **8A,B** (and **Fig. S33**), emission spectra show similar signatures for all the samples, with a maximum
516 at *ca.* $\lambda_{em} = 405$ nm, associated with an emission band in the $\lambda_{ex} = 350-370$ nm-range. These

517 characteristic excitation/emission wavelengths have already been reported for the excitation
518 exchanges between phenylalanine rings involved in intermolecular π - π interactions,^{63,107,108}
519 confirming that the phenylalanines of the peptide part play pivotal roles in the supramolecular
520 assembly process (*nota*: this excitation peak is heightened for the **p(TG)-FEFK + FEFK** mixture
521 (**Fig. S33**), in which Phe stacking are predominant). Interestingly, another contribution has been
522 observed, with a characteristic excitation peak at *ca.* 315 nm, corresponding to stacking
523 associations of nucleic acids in water, confirming that PNA nucleobases interact each other in the
524 supramolecular assembly, with an exacerbated peak for the **p(TG)-FEFK + p(AC)-FEFK** (**Fig.**
525 **7A**), *i.e.*, the mixture with nucleopeptides containing the complementary nucleobases. These results
526 are not surprising because in DNA, for instance, the double helix is, of course, stabilized by
527 hydrogen bonds between complementary nucleobases, but also by π -stacking interactions between
528 the adjacent nucleobases of a same strand.^{109,110} We can thus argue that the PNA parts of the
529 nucleopeptides interact, *inter alia*, via stacking interactions, has already reported by our group^{63,67}
530 and others.^{62,111} Interestingly, all these mixtures (**Fig. 8C** and **Fig. S34**) exhibit a red-edge
531 excitation shift (REES),¹¹² originating from the slowdown of the solvent dielectric relaxation
532 process due to water molecules trapped in the hydrogel scaffold (*i.e.*, inside and/or in interaction
533 with fibrils and/or other nanoobjects, *vide supra*) and in interactions with fluorophores (*i.e.*,
534 phenylalanine and PNA moieties herein).^{67,111,113} This peculiar intrinsic optical property, mainly
535 observed for polymers, allows to modulate the emission wavelength depending of the applied
536 excitation wavelength, and can be considered for biophysical and nanotechnological
537 applications.^{112,114-116} Thus, we observed (**Fig. 8C,D** and **Fig. S34**) a greater REES for the mixture
538 **p(TG)-FEFK + p(AC)-FEFK** containing the complementary nucleobase sequences (slope =
539 0.91), than for the mixture containing one (*i.e.*, **p(TG)-FEFK + p(CC)-FEFK** with slope = 0.78)
540 and two mismatches (*i.e.*, **p(TG)-FEFK + p(CC)-FEFK** with slope = 0.37), which can be

541 explained by a higher organized structure for the first one than for the other two (in accordance
542 with other data, including microscopies, discussed *vide supra*).

543 To get further insights into the actual mode of interaction of the nucleobase moieties into
544 supramolecular assembly process, we performed NMR High-Resolution Magic Angle Spinning
545 (HR-MAS) experiments, a powerful but still little-used method for the study of peptide derivative-
546 based hydrogels,^{88,117} directly on the hydrogel exhibiting the highest synergistic effects, *i.e.*, on the
547 equimolar mixture **p(AC)-FEFK** + **p(TG)-FEFK** (15 mM, Tris-d₁₁.HCl, pH 7.4). Interestingly,
548 while no signal is observed in the 10-14 ppm region for each compound alone in solution, the
549 mixture (in red, **Fig. 9A,C**) exhibits two characteristic sets of signals at 13.55 ppm, assigned to the
550 imido proton of the thymine, and in the 10.5-13 ppm range, assigned to the imino proton of the
551 guanine.¹¹⁸ The presence of these peaks means that the exchange rates of these protons are slowed
552 down upon mixing the two complementary nucleopeptides, which can be explained by the
553 involvement of these protons in hydrogen bonds, *i.e.*, in the formation of base pairings (**Fig. 9B**).¹¹⁸
554 Thus, while requiring further investigations, these data support that the complementary nucleobase-
555 containing PNA moieties thymine-guanine (in **p(TG)-FEFK**) and adenine-cytosine (in **p(AC)-**
556 **FEFK**) co-assemble *via* the formation of intermolecular thymine/adenine and guanine/cytosine
557 base pairings (as proposed **Fig. 1B**). Such interactions, observed with TO fluorescence (*vide*
558 *supra*), have recently been reported for nucleopeptide interactions thanks to computational
559 modelling,^{62,75} and can explain the highly synergistic mechanical and physicochemical properties
560 observed and discussed hereinbefore, confirming the value of the design of this new series of
561 nucleopeptides discussed herein.

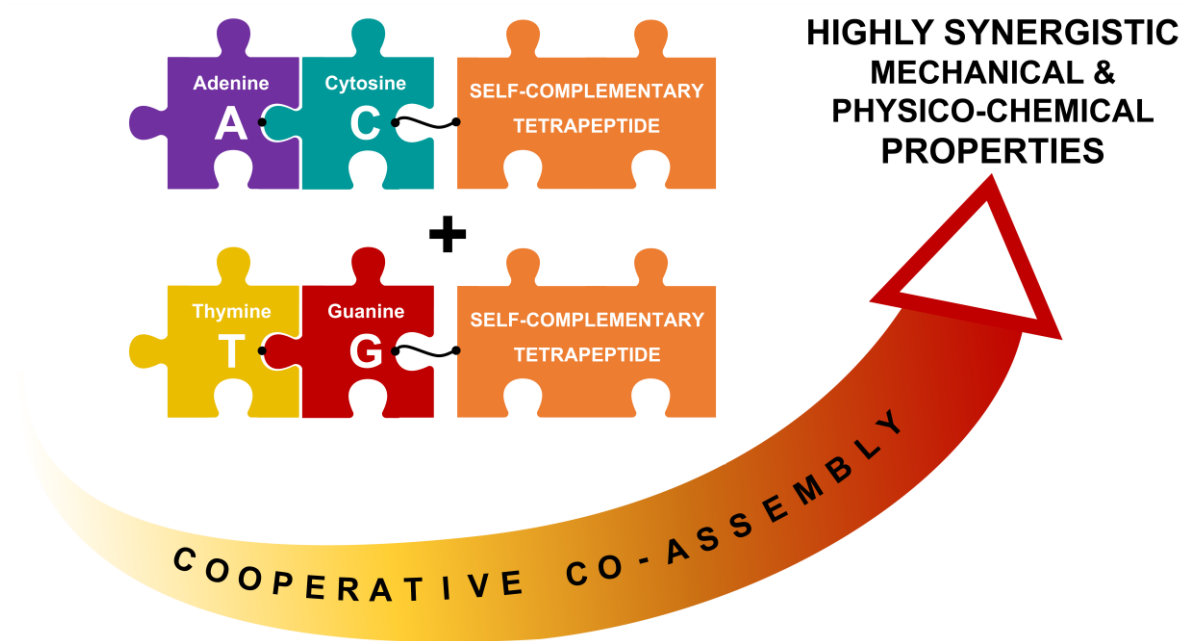
562

563 **CONCLUSIONS**

564 While the overwhelming majority of peptide derivative-based hydrogels has been developed from
565 one and only one compound through a mono-component approach leading to numerous limitations,
566 we successfully reported herein on a new multicomponent system exhibiting high efficiency (with
567 storage moduli up to 720 kPa) and high synergistic (physicochemical and mechanical) properties.
568 Indeed, the new series of nucleopeptides we developed demonstrates cooperative effects, mainly
569 when the two complementary p(TG)-FEFK and p(AC)-FEFK, designed with self-complementary
570 peptide sequences and complementary nucleobase-containing moieties, are mixed. Thus, hydrogel
571 stiffness and resistance to external stress can be significantly improved by a factor of > 2700 and
572 > 37, respectively, far better than for nucleopeptides alone and for the mixtures in which
573 nucleopeptides comprised nucleobase mismatches. Thanks to a multiscale approach, we
574 highlighted that such synergy originates from the formation of specific interactions between the
575 peptide parts (*via* the formation of β -sheet (ThT fluorescence, CD, FTIR) and π -stacking
576 interactions (fluorescence)) and between the nucleobase-containing moieties (*via* hydrogen bonds
577 thanks to base pairing (HR-MAS NMR and TO experiments) and π -stacking interactions
578 (fluorescence)). These supramolecular interactions led to the formation of a dense fibrillar network
579 able to self-organize into a porous hydrogel scaffold with homogeneous alveoli (cryo-SEM, TEM)
580 offering high capability to entrap water molecules. Altogether, these data highlight the high
581 potential of nucleopeptides, considered as emerging and of high interest for the formation of low-
582 molecular weight hydrogels,⁵⁶ to design multicomponent supramolecular hydrogels with high
583 synergistic effects and offering a large range of mechanical and physicochemical properties
584 difficult to obtain with a monocomponent approach, thanks to their dual nucleic/peptide nature.

585

586

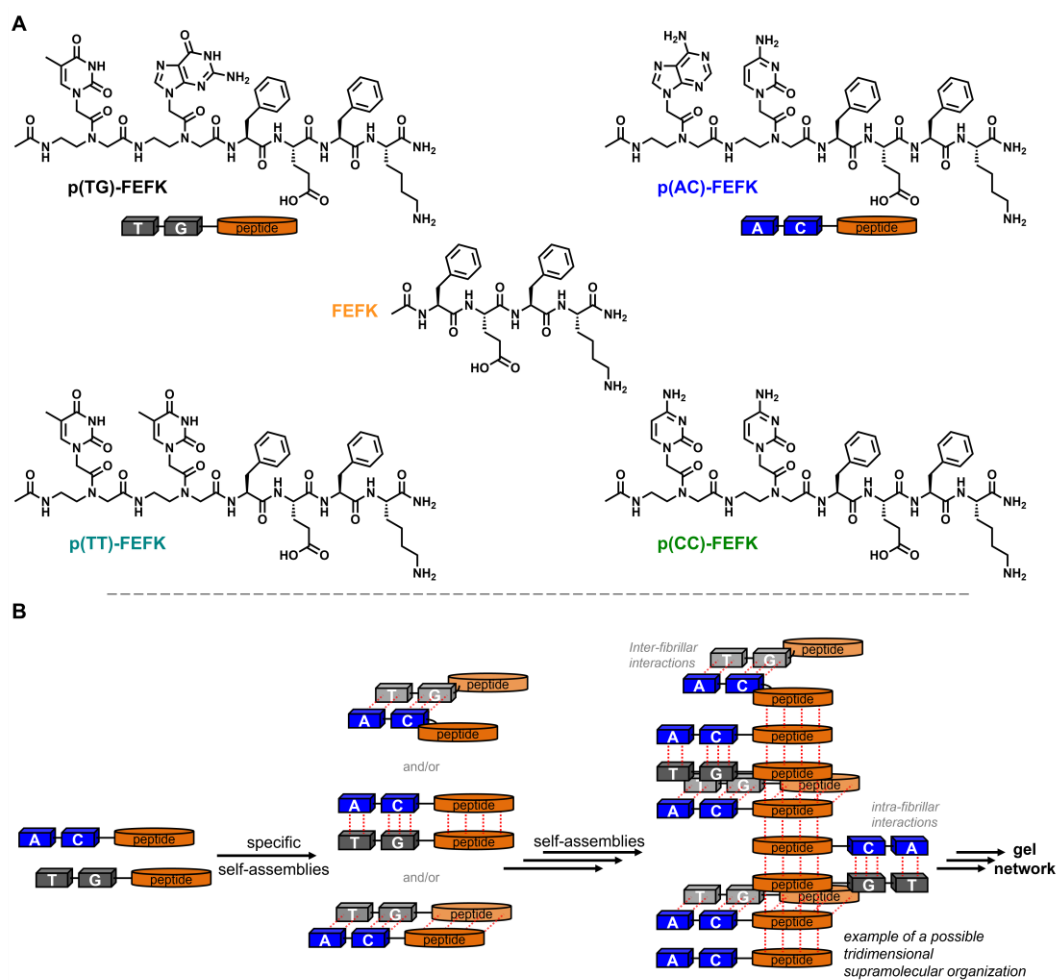


588

589

TOC

590



591

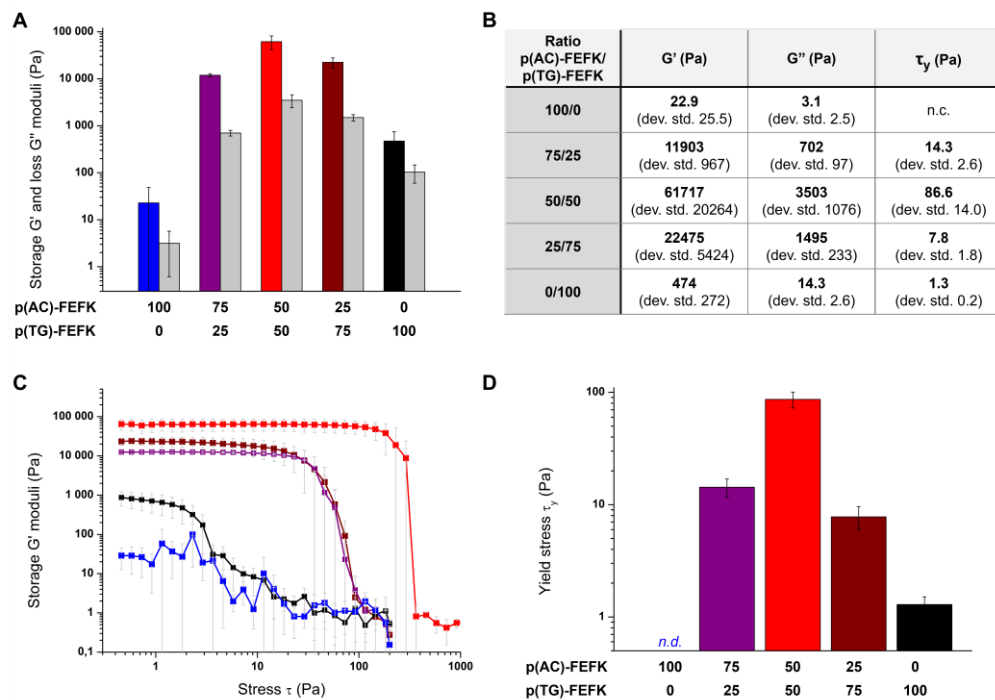
592 **Figure 1.** (A) (top) Chemical structures of the two main nucleopeptides p(TG)-FEFK and p(AC)-

593 FEFK incorporating ionic auto-complementary peptide sequences and complementary nucleobase

594 sequences (*i.e.*, TG vs AC), and control compounds. (B) Schematic representation of the expected

595 supramolecular assemblies based on specific peptide and/or nucleobase interactions.

596

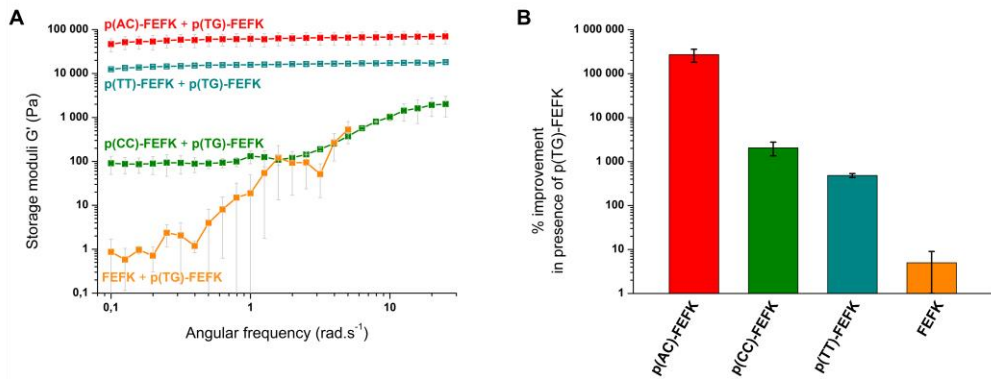


597

598 **Figure 2.** Rheological studies of the p(AC)-FEFK and p(TG)-FEFK mixtures at different ratio
 599 showing: (A) the evolution of the storage (G') and loss (G'' , in grey) moduli (characteristic values
 600 are reported in B), (C) the different resistances of the gels as a function of mechanical stress and
 601 (D) the characteristic limiting values of the linear viscoelastic region (yield stress τ_y).

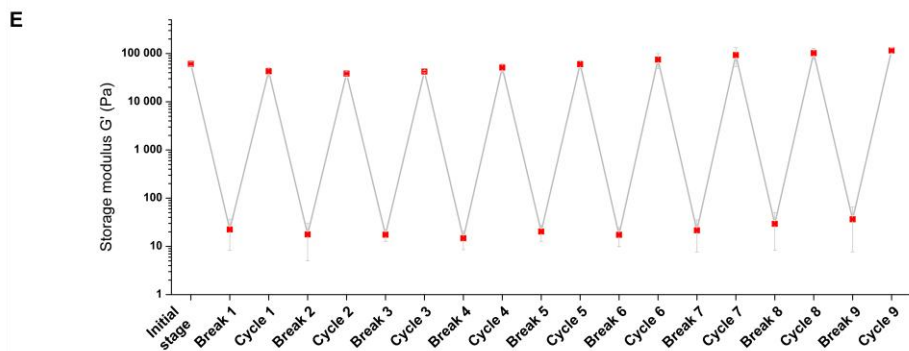
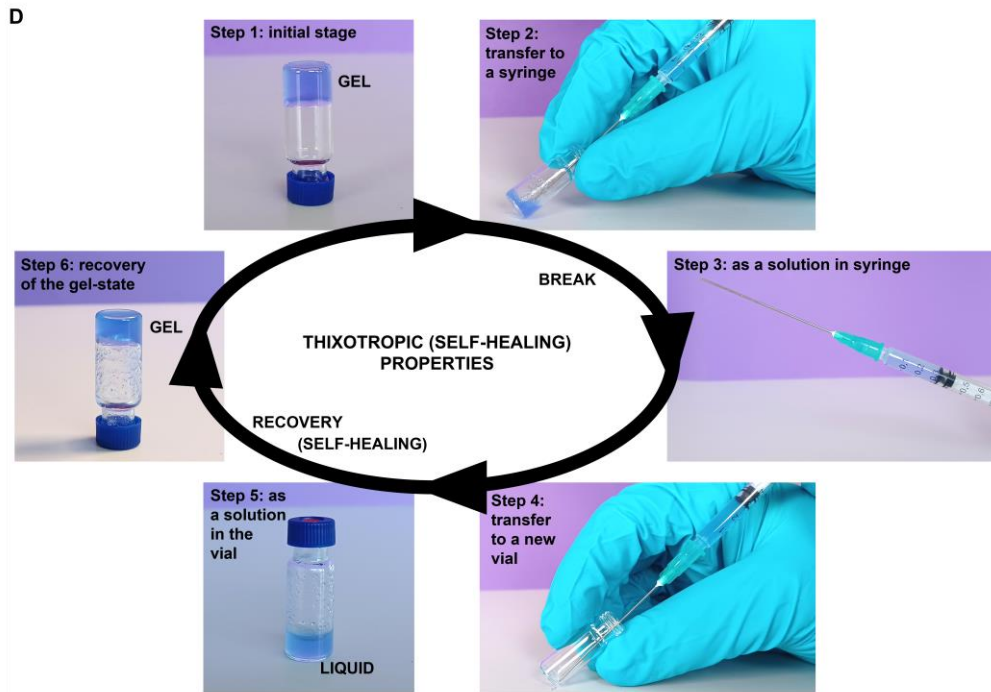
602

603



C

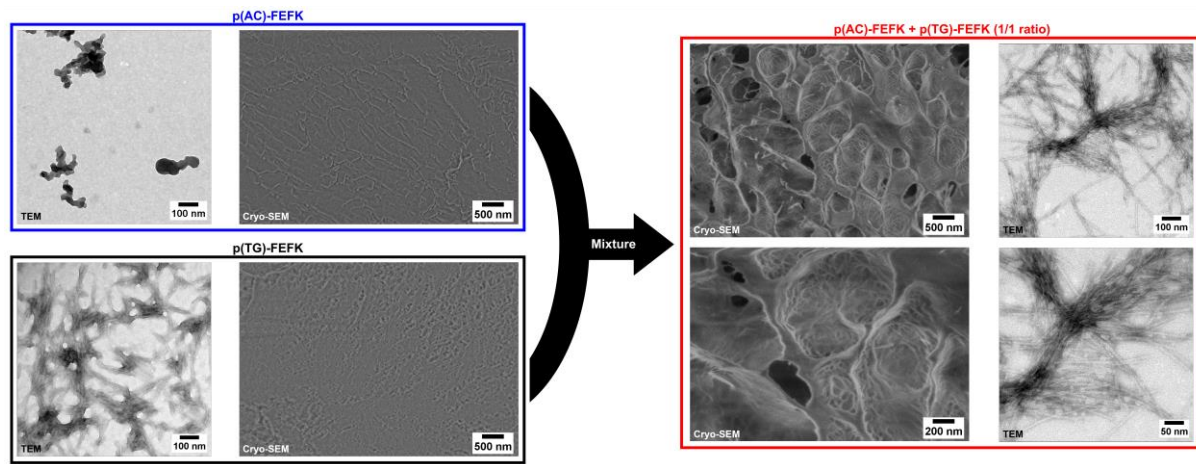
(Nucleo)peptide	G' (Pa) alone	G' (Pa) with p(TG)-FEFK (1/1 ratio)	Ratio G' with/ G' without p(TG)-FEFK	%Improvement
p(AC)-FEFK	22.9 Pa (dev. std. 25.5)	61 717 Pa (dev. std. 20 264)	2707 (dev. std. 888)	+270 600% (dev. std. 88 800)
p(CC)-FEFK	6.1 Pa (dev. std. 8.1)	131.8 Pa (dev. std. 43.2)	21.6 (dev. std. 7.1)	+2 060% (dev. std. 710)
p(TT)-FEFK	2713 Pa (dev. std. 432)	15 840 Pa (dev. std. 1245)	5.8 (dev. std. 0.5)	+484% (dev. std. 50)
FEFK	18.9 Pa (dev. std. 16.9)	19.9 Pa (dev. std. 19.3)	1.0 (dev. std. 0.9)	+5% (dev. std. 4)



605 **Figure 3.** (A) Frequency sweep experiments of **p(TG)-FEFK** in the presence of **p(AC)-FEFK**
606 (red), **p(CC)-FEFK** (green), **p(TT)-FEFK** (dark cyan) and **FEFK** (orange). (B) Percentage
607 improvement of the storage moduli of the nucleopeptide and peptide derivatives in the presence of
608 **p(TG)-FEFK** (see **Fig. S6**), and (C) characteristic values reported. The equimolar **p(AC)-FEFK**
609 + **p(TG)-FEFK** mixture exhibits thixotropic properties allowing several transfer cycles to a
610 syringe (D) while maintaining its mechanical properties, as confirmed by rheology (E).

611

612

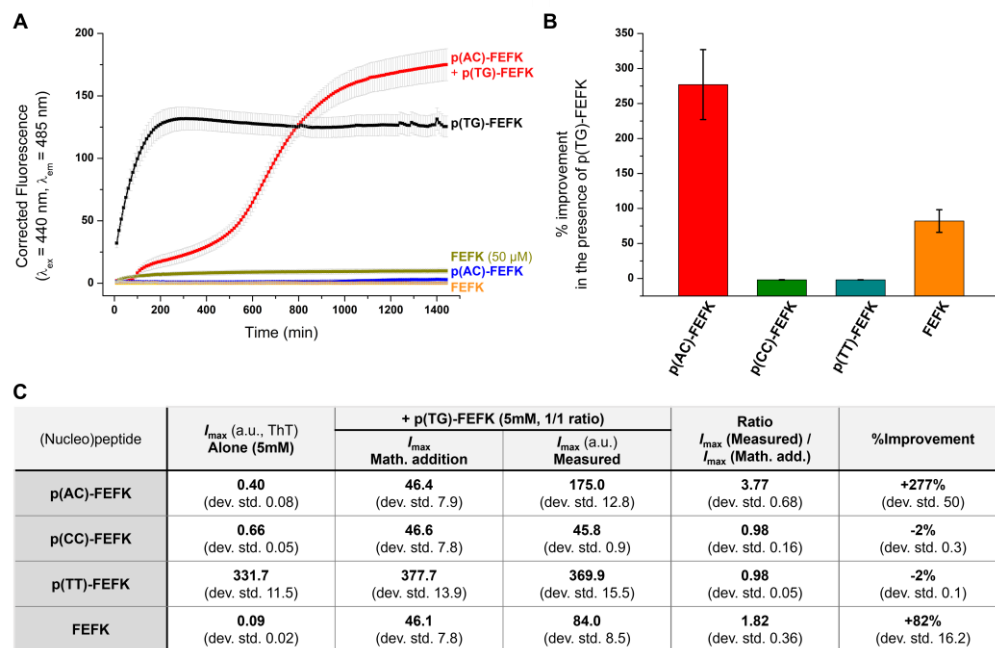


613

614 **Figure 4.** Cryo-SEM and TEM images obtained for p(AC)-FEFK and p(TG)-FEFK alone (left
615 panel) and for their equimolar mixture (right panel) at 15 mM (Tris.HCl, pH 7.4). TEM were
616 recorded with negative staining by phosphotungstic acid.

617

618



619

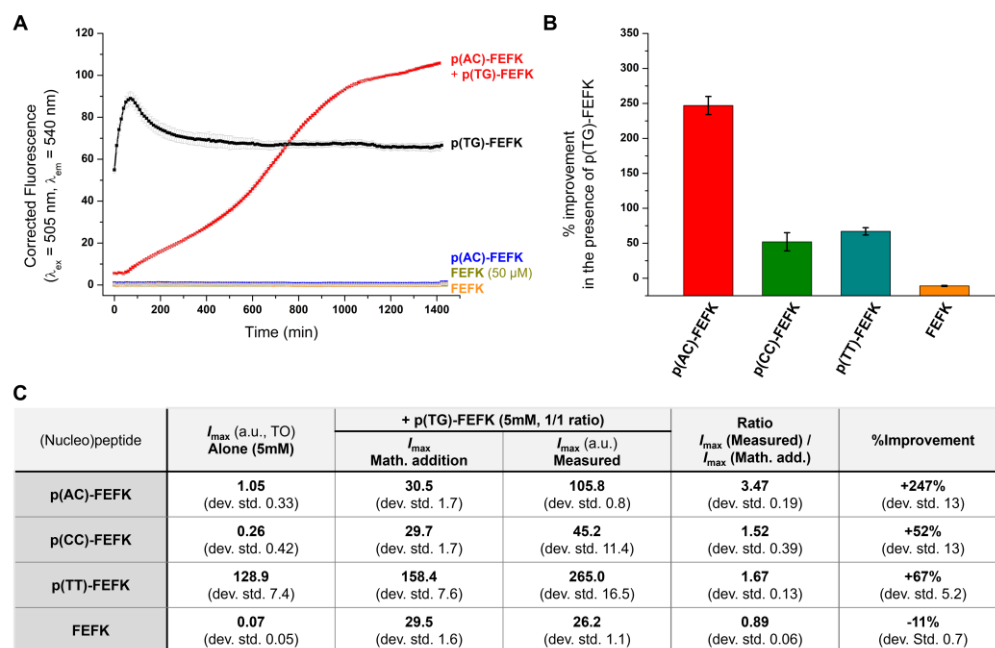
620 **Figure 5.** (A) Fibril formation monitored by Thioflavin T fluorescence assay (ThT, $\lambda_{ex}/\lambda_{em} =$

621 440/485 nm, 10 mM total concentration) as a function of time. (B) Plot of the percentage

622 improvement of the maximum fluorescence intensity of the nucleopeptide and peptide derivatives

623 in the presence of p(TG)-FEFK (see also Fig S22), reported in the table (C).

624



625

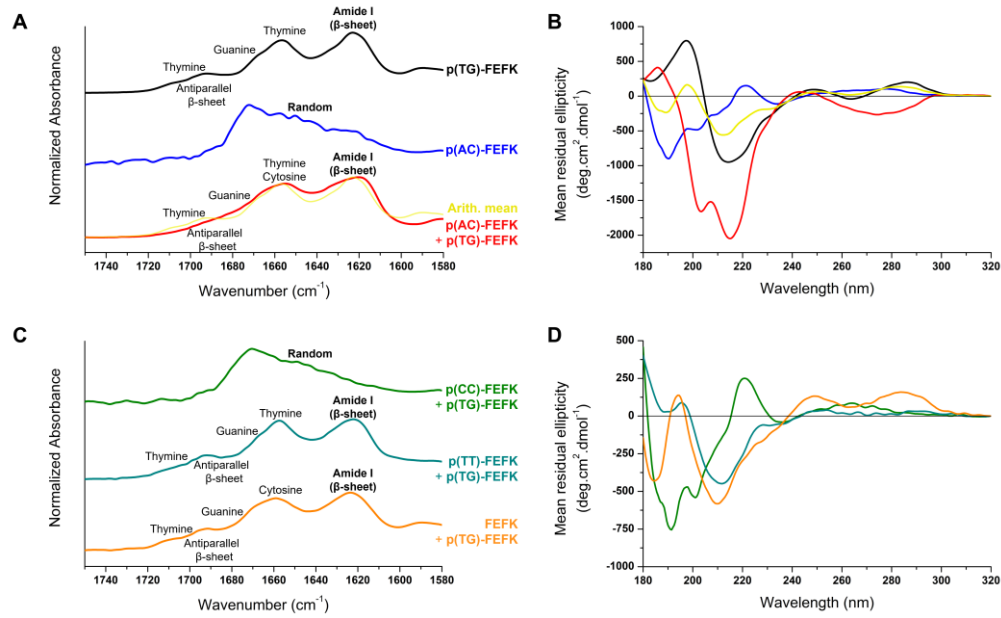
626 **Figure 6. (A)** Nucleobase interactions monitored by Thiazole Orange fluorescence assay (TO,

627 $\lambda_{ex}/\lambda_{em} = 505/540 \text{ nm}$, 10 mM total concentration) as a function of time. **(B)** Plot of the

628 percentage improvement of the maximum fluorescence intensity of the nucleopeptide and peptide

629 derivatives in the presence of **p(TG)-FEFK**(see also **Fig S24**), reported in the table (C).

630



631

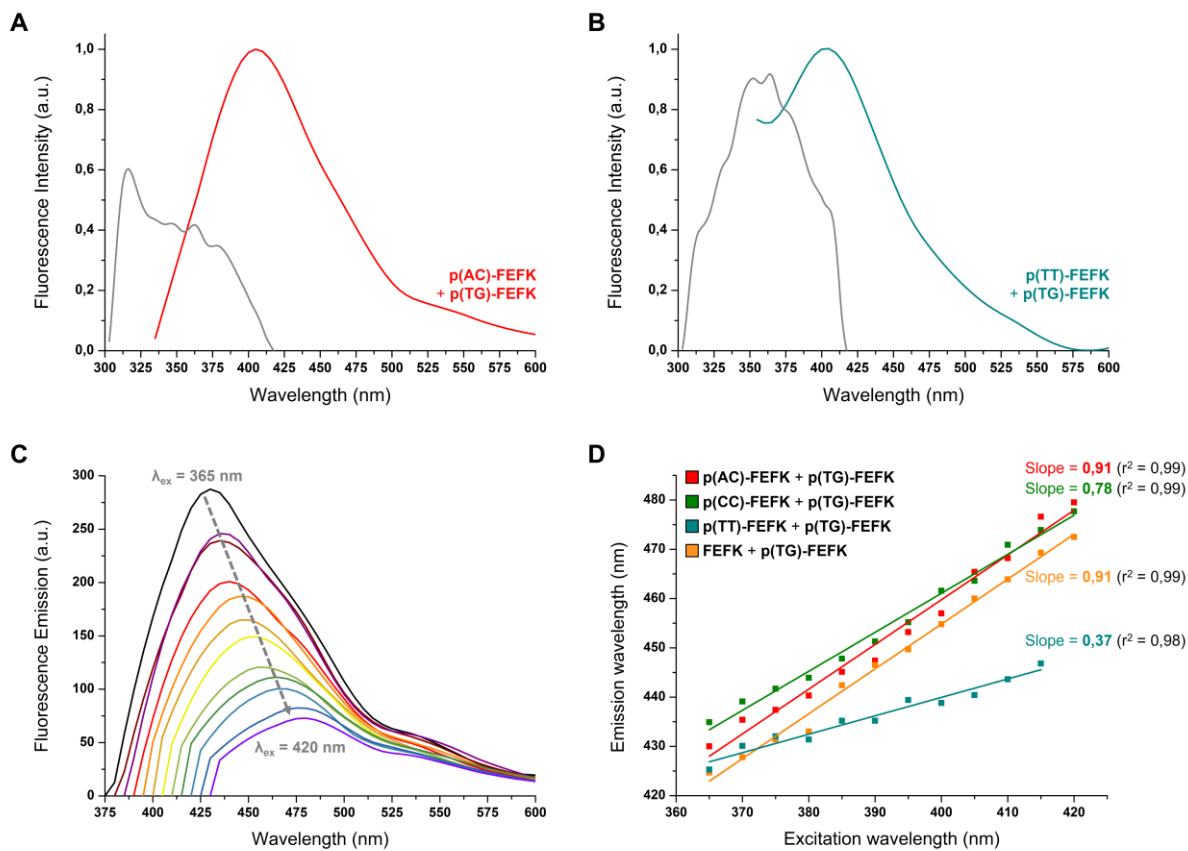
632 **Figure 7.** FTIR (A, C) and circular dichroism (B, D) spectra of (nucleo)peptides alone and of

633 equimolar mixtures (the same color code is used for A and B, and for C and D). The dark yellow

634 spectra in A,B corresponds to the arithmetic mean of the 1/1 p(AC)-FEFK/p(TG)-FEFK

635 mixture.

636

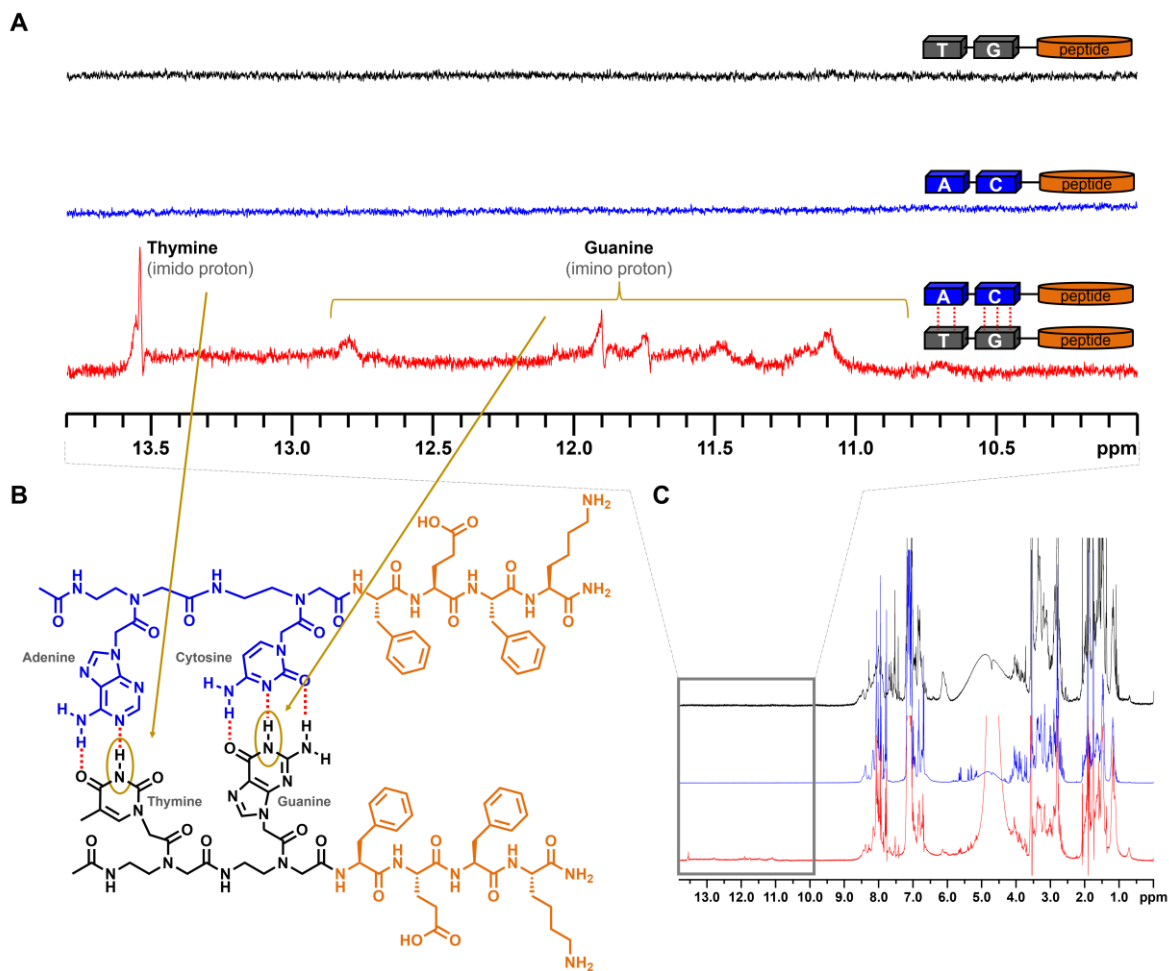


637
 638 **Figure 8.** (A,B) Emission (in color) and excitation (in grey) spectra at $\lambda_{ex} = 316$ nm and $\lambda_{em} =$
 639 422 nm. (C) Evolution of the fluorescence emission spectra as a function of the excitation
 640 wavelength (from 365 nm to 420nm) which exhibit a red-edge shift characterized by (D) a linear
 641 correlation between the emission and excitation wavelengths.

642

643

644



645

646 **Figure 9.** NMR spectra ((A) Full and (C) Enlargement of the 10-14 ppm region) of **p(TG)-FEFK**

647 (in black) and **p(AC)-FEFK** (in blue) alone at 7.5mM, and their equimolar mixture (15mM, in red)

648 measured by High Resolution Magic Angle Spinning (HR-MAS) NMR, in buffer Tris- d_{11} .HCl, pH

649 7.4. While absent for the compounds alone, a set of characteristic peaks appears between 10.5 ppm

650 and 13.5 ppm, attributed to the imido and imino protons of the thymine and guanine moiety,

651 respectively, involved in hydrogen bonds, as proposed in (B).

652

653

654 ASSOCIATED CONTENT

655 **Supporting information.**

656 Chemical characterization of synthesized peptides and additional data (rheology, electron
657 microscopies, FTIR, fluorescence and CD) are available in the Supporting Information.

658

659 AUTHOR INFORMATION

660 **Corresponding Author**

661 Loic Stefan – Université de Lorraine, CNRS, LCPM, F-54000 Nancy, France; Email:

662 loic.stefan@univ-lorraine.fr

663 **Funding Sources**

664 Agence Nationale de la Recherche (ANR-20-CE06-0010-01 MUNCH)

665

666 ACKNOWLEDGEMENT

667 L. S. and M.-C. A.-P. acknowledge the Centre National de la Recherche Scientifique (CNRS) for
668 fundings. L. S. and P. H. thank the Agence Nationale de la Recherche (ANR-20-CE06-0010-01
669 MUNCH) for funding. The authors thank Mathilde Achard for technical support on peptide
670 synthesis and purification, Marc Schmutz for discussions on electron microscopy, Sylvie Migot for
671 TEM analyses, and the UMS 2008 IBSLor (for CD), MassLor (for HRMS), CC3M (for TEM) and
672 APPEL (LCPM, Université de Lorraine, for access to NMR, FTIR and HPLC) facilities.

673

674 REFERENCES

- 675 (1) Yu, L.; Dean, K.; Li, L. Polymer Blends and Composites from Renewable Resources.
676 *Prog. Polym. Sci.* **2006**, 576–602. <https://doi.org/10.1016/j.progpolymsci.2006.03.002>.
- 677 (2) Koning, C.; Van Duin, M.; Pagnoulle, C.; Jerome, R. Strategies for Compatibilization of
678 Polymer Blends. *Prog. Polym. Sci.* **1998**, 707–757. <https://doi.org/10.1016/S0079->
679 6700(97)00054-3.
- 680 (3) Miracle, D. B.; Senkov, O. N. A Critical Review of High Entropy Alloys and Related
681 Concepts. *Acta Mater.* **2017**, 122, 448–511. <https://doi.org/10.1016/j.actamat.2016.08.081>.
- 682 (4) Feng, L.; Wang, K. Y.; Day, G. S.; Zhou, H. C. The Chemistry of Multi-Component and
683 Hierarchical Framework Compounds. *Chem. Soc. Rev.* **2019**, 48, 4823–4853.
684 <https://doi.org/10.1039/c9cs00250b>.
- 685 (5) De Leon Rodriguez, L. M.; Hemar, Y.; Cornish, J.; Brimble, M. A. Structure-Mechanical
686 Property Correlations of Hydrogel Forming β -Sheet Peptides. *Chem. Soc. Rev.* **2016**, 45,
687 4797–4824. <https://doi.org/10.1039/c5cs00941c>.
- 688 (6) Levin, A.; Hakala, T. A.; Schnaider, L.; Bernardes, G. J. L.; Gazit, E.; Knowles, T. P. J.
689 Biomimetic Peptide Self-Assembly for Functional Materials. *Nat. Rev. Chem.* **2020**, 4,
690 615–634. <https://doi.org/10.1038/s41570-020-0215-y>.
- 691 (7) Mondal, S.; Das, S.; Nandi, A. K. A Review on Recent Advances in Polymer and Peptide
692 Hydrogels. *Soft Matter* **2020**, 16, 1404–1454. <https://doi.org/10.1039/c9sm02127b>.
- 693 (8) Das, R.; Gayakvad, B.; Shinde, S. D.; Rani, J.; Jain, A.; Sahu, B. Ultrashort Peptides - A
694 Glimpse into the Structural Modifications and Their Applications as Biomaterials. *ACS*

- 695 *Appl. Bio Mater.* **2020**, *3*, 5474–5499. <https://doi.org/10.1021/acsabm.0c00544>.
- 696 (9) Okesola, B. O.; Mata, A. Multicomponent Self-Assembly as a Tool to Harness New
697 Properties from Peptides and Proteins in Material Design. *Chem. Soc. Rev.* **2018**, *47*,
698 3721–3736. <https://doi.org/10.1039/c8cs00121a>.
- 699 (10) Raymond, D. M.; Nilsson, B. L. Multicomponent Peptide Assemblies. *Chem. Soc. Rev.*
700 **2018**, *47*, 3659–3720. <https://doi.org/10.1039/c8cs00115d>.
- 701 (11) Makam, P.; Gazit, E. Minimalistic Peptide Supramolecular Co-Assembly: Expanding the
702 Conformational Space for Nanotechnology. *Chem. Soc. Rev.* **2018**, *47*, 3406–3420.
703 <https://doi.org/10.1039/c7cs00827a>.
- 704 (12) Seliktar, D. Designing Cell-Compatible Hydrogels for Biomedical Applications. *Science*
705 **2012**, *336*, 1124–1128. <https://doi.org/10.1126/science.1214804>.
- 706 (13) Seow, W. Y.; Hauser, C. A. E. Short to Ultrashort Peptide Hydrogels for Biomedical Uses.
707 *Mater. Today* **2014**, *17*, 381–388. <https://doi.org/10.1016/j.mattod.2014.04.028>.
- 708 (14) Dou, X. Q.; Feng, C. L. Amino Acids and Peptide-Based Supramolecular Hydrogels for
709 Three-Dimensional Cell Culture. *Adv. Mater.* **2017**, *29*, 1604062.
710 <https://doi.org/10.1002/adma.201604062>.
- 711 (15) Das, A. K.; Gavel, P. K. Low Molecular Weight Self-Assembling Peptide-Based Materials
712 for Cell Culture, Antimicrobial, Anti-Inflammatory, Wound Healing, Anticancer, Drug
713 Delivery, Bioimaging and 3D Bioprinting Applications. *Soft Matter* **2020**, *16*, 10065–
714 10095. <https://doi.org/10.1039/d0sm01136c>.
- 715 (16) Li, J.; Xing, R.; Bai, S.; Yan, X. Recent Advances of Self-Assembling Peptide-Based

- 716 Hydrogels for Biomedical Applications. *Soft Matter*. **2019**, *15*, 1704–1715.
717 <https://doi.org/10.1039/C8SM02573H>.
- 718 (17) Sato, K.; Hendricks, M. P.; Palmer, L. C.; Stupp, S. I. Peptide Supramolecular Materials
719 for Therapeutics. *Chem. Soc. Rev.* **2018**, *47*, 7539–7551.
720 <https://doi.org/10.1039/c7cs00735c>.
- 721 (18) De Santis, E.; Ryadnov, M. G. Peptide Self-Assembly for Nanomaterials: The Old New
722 Kid on the Block. *Chem. Soc. Rev.* **2015**, *44*, 8288–8300.
723 <https://doi.org/10.1039/c5cs00470e>.
- 724 (19) Stefan, L. Amino Acids Modification to Improve and Fine-Tune Peptide- Based
725 Hydrogels. In *Amino Acid - New Insights and Roles in Plant and Animal*; Asao, T.,
726 Asaduzzaman, M., Eds.; IntechOpen, 2017; pp 31–73.
727 <https://doi.org/10.5772/intechopen.68705>.
- 728 (20) Du, X.; Zhou, J.; Shi, J.; Xu, B. Supramolecular Hydrogelators and Hydrogels: From Soft
729 Matter to Molecular Biomaterials. *Chem. Rev.* **2015**, *115*, 13165–13307.
730 <https://doi.org/10.1021/acs.chemrev.5b00299>.
- 731 (21) Grzybowski, B. A.; Huck, W. T. S. The Nanotechnology of Life-Inspired Systems. *Nat.*
732 *Nanotechnol.* **2016**, *11*, 585–592. <https://doi.org/10.1038/nnano.2016.116>.
- 733 (22) Li, L.; Sun, R.; Zheng, R. Tunable Morphology and Functionality of Multicomponent Self-
734 Assembly: A Review. *Mater. Des.* **2021**, *197*, 109209.
735 <https://doi.org/10.1016/j.matdes.2020.109209>.
- 736 (23) Hsu, S. M.; Wu, F. Y.; Lai, T. S.; Lin, Y. C.; Lin, H. C. Self-Assembly and Hydrogelation
737 from Multicomponent Coassembly of Pentafluorobenzyl-Phenylalanine and

- 738 Pentafluorobenzyl-Diphenylalanine. *RSC Adv.* **2015**, *5*, 22943–22946.
739 <https://doi.org/10.1039/c5ra01020a>.
- 740 (24) Ghosh, M.; Bera, S.; Schiffmann, S.; Shimon, L. J. W.; Adler-Abramovich, L. Collagen-
741 Inspired Helical Peptide Coassembly Forms a Rigid Hydrogel with Twisted Polyproline II
742 Architecture. *ACS Nano* **2020**, *14*, 9990–10000. <https://doi.org/10.1021/acsnano.0c03085>.
- 743 (25) Draper, E. R.; Wallace, M.; Schweins, R.; Poole, R. J.; Adams, D. J. Nonlinear Effects in
744 Multicomponent Supramolecular Hydrogels. *Langmuir* **2017**, *33*, 2387–2395.
745 <https://doi.org/10.1021/acs.langmuir.7b00326>.
- 746 (26) Du, E. Y.; Ziaee, F.; Wang, L.; Nordon, R. E.; Thordarson, P. The Correlations between
747 Structure, Rheology, and Cell Growth in Peptide-Based Multicomponent Hydrogels.
748 *Polym. J.* **2020**, *52*, 947–957. <https://doi.org/10.1038/s41428-020-0351-8>.
- 749 (27) Diaferia, C.; Ghosh, M.; Sibillano, T.; Gallo, E.; Stornaiuolo, M.; Giannini, C.; Morelli,
750 G.; Adler-Abramovich, L.; Accardo, A. Fmoc-FF and Hexapeptide-Based Multicomponent
751 Hydrogels as Scaffold Materials. *Soft Matter* **2019**, *15*, 487–496.
752 <https://doi.org/10.1039/c8sm02366b>.
- 753 (28) Gao, J.; Tang, C.; Elsayy, M. A.; Smith, A. M.; Miller, A. F.; Saiani, A. Controlling Self-
754 Assembling Peptide Hydrogel Properties through Network Topology. *Biomacromolecules*
755 **2017**, *18*, 826–834. <https://doi.org/10.1021/acs.biomac.6b01693>.
- 756 (29) Gila-Vilchez, C.; Mañas-Torres, M. C.; González-Vera, J. A.; Franco-Montalban, F.;
757 Tamayo, J. A.; Conejero-Lara, F.; Cuerva, J. M.; Lopez-Lopez, M. T.; Orte, A.; Álvarez
758 De Cienfuegos, L. Insights into the Co-Assemblies Formed by Different Aromatic Short-
759 Peptide Amphiphiles. *Polym. Chem.* **2021**, *12*, 6832–6845.

760 <https://doi.org/10.1039/d1py01366a>.

761 (30) Ardon, H. A. M.; Draper, E. R.; Citossi, F.; Wallace, M.; Serpell, L. C.; Adams, D. J.;
762 Tovar, J. D. Kinetically Controlled Coassembly of Multichromophoric Peptide
763 Hydrogelators and the Impacts on Energy Transport. *J. Am. Chem. Soc.* **2017**, *139*, 8685–
764 8692. <https://doi.org/10.1021/jacs.7b04006>.

765 (31) Xing, P.; Chen, H.; Xiang, H.; Zhao, Y. Selective Coassembly of Aromatic Amino Acids
766 to Fabricate Hydrogels with Light Irradiation-Induced Emission for Fluorescent Imprint.
767 *Adv. Mater.* **2018**, *30*, 1705633. <https://doi.org/10.1002/adma.201705633>.

768 (32) Khalily, M. A.; Bakan, G.; Kucukoz, B.; Topal, A. E.; Karatay, A.; Yaglioglu, H. G.;
769 Dana, A.; Guler, M. O. Fabrication of Supramolecular n/p-Nanowires via Coassembly of
770 Oppositely Charged Peptide-Chromophore Systems in Aqueous Media. *ACS Nano* **2017**,
771 *11*, 6881–6892. <https://doi.org/10.1021/acsnano.7b02025>.

772 (33) Chia, J. Y.; Miki, T.; Mihara, H.; Tsutsumi, H. Biofunctional Supramolecular Hydrogels
773 Fabricated from a Short Self-Assembling Peptide Modified with Bioactive Sequences for
774 the 3D Culture of Breast Cancer MCF-7 Cells. *Bioorganic Med. Chem.* **2021**, *46*, 116345.
775 <https://doi.org/10.1016/j.bmc.2021.116345>.

776 (34) Tajima, A.; Liu, W.; Pradhan, I.; Bertera, S.; Bagia, C.; Trucco, M.; Meng, W. S.; Fan, Y.
777 Bioengineering Mini Functional Thymic Units with EAK16-II/EAKIIIH6 Self-Assembling
778 Hydrogel. *Clin. Immunol.* **2015**, *160*, 82–89. <https://doi.org/10.1016/j.clim.2015.03.010>.

779 (35) Cigognini, D.; Satta, A.; Colleoni, B.; Silva, D.; Donegà, M.; Antonini, S.; Gelain, F.
780 Evaluation of Early and Late Effects into the Acute Spinal Cord Injury of an Injectable
781 Functionalized Self-Assembling Scaffold. *PLoS One* **2011**, *6*, e19782.

- 782 <https://doi.org/10.1371/journal.pone.0019782>.
- 783 (36) Sahoo, J. K.; Vandenberg, M. A.; Ruiz Bello, E. E.; Nazareth, C. D.; Webber, M. J.
784 Electrostatic-Driven Self-Sorting and Nanostructure Speciation in Self-Assembling
785 Tetrapeptides. *Nanoscale* **2019**, *11*, 16534–16543. <https://doi.org/10.1039/c9nr03440d>.
- 786 (37) Tena-Solsona, M.; Alonso-De Castro, S.; Miravet, J. F.; Escuder, B. Co-Assembly of
787 Tetrapeptides into Complex PH-Responsive Molecular Hydrogel Networks. *J. Mater.*
788 *Chem. B* **2014**, *2*, 6192–6197. <https://doi.org/10.1039/c4tb00795f>.
- 789 (38) Panja, S.; Dietrich, B.; Shebanova, O.; Smith, A. J.; Adams, D. J. Programming Gels Over
790 a Wide PH Range Using Multicomponent Systems. *Angew. Chemie - Int. Ed.* **2021**, *60*,
791 9973–9977. <https://doi.org/10.1002/anie.202101247>.
- 792 (39) Wang, D.; Hou, X.; Zhang, X.; Zhao, Y.; Ma, B.; Sun, Y.; Wang, J. Light-A Nd PH-
793 Controlled Hierarchical Coassembly of Peptide Amphiphiles. *Langmuir* **2019**, *35*, 9841–
794 9847. <https://doi.org/10.1021/acs.langmuir.9b01459>.
- 795 (40) Thota, C. K.; Berger, A. A.; Elomaa, L.; Nie, C.; Böttcher, C.; Kokschi, B. Coassembly
796 Generates Peptide Hydrogel with Wound Dressing Material Properties. *ACS Omega* **2020**,
797 *5*, 8557–8563. <https://doi.org/10.1021/acsomega.9b04371>.
- 798 (41) Afami, M. E.; El Karim, I.; About, I.; Krasnodembskaya, A. D.; Laverty, G.; Lundy, F. T.
799 Multicomponent Peptide Hydrogels as an Innovative Platform for Cell-Based Tissue
800 Engineering in the Dental Pulp. *Pharmaceutics* **2021**, *13*, 1575.
801 <https://doi.org/10.3390/pharmaceutics13101575>.
- 802 (42) Pal, V. K.; Jain, R.; Roy, S. Tuning the Supramolecular Structure and Function of
803 Collagen Mimetic Ionic Complementary Peptides via Electrostatic Interactions. *Langmuir*

- 804 **2020**, *36*, 1003–1013. <https://doi.org/10.1021/acs.langmuir.9b02941>.
- 805 (43) King, P. J. S.; Giovanna Lizio, M.; Booth, A.; Collins, R. F.; Gough, J. E.; Miller, A. F.;
806 Webb, S. J. A Modular Self-Assembly Approach to Functionalised β -Sheet Peptide
807 Hydrogel Biomaterials. *Soft Matter* **2016**, *12*, 1915–1923.
808 <https://doi.org/10.1039/c5sm02039e>.
- 809 (44) Liyanage, W.; Vats, K.; Rajbhandary, A.; Benoit, D. S. W.; Nilsson, B. L.
810 Multicomponent Dipeptide Hydrogels as Extracellular Matrix-Mimetic Scaffolds for Cell
811 Culture Applications. *Chem. Commun.* **2015**, *51*, 11260–11263.
812 <https://doi.org/10.1039/c5cc03162a>.
- 813 (45) Giuri, D.; Marshall, L. J.; Dietrich, B.; McDowall, D.; Thomson, L.; Newton, J. Y.;
814 Wilson, C.; Schweins, R.; Adams, D. J. Exploiting and Controlling Gel-to-Crystal
815 Transitions in Multicomponent Supramolecular Gels. *Chem. Sci.* **2021**, *12*, 9720–9725.
816 <https://doi.org/10.1039/d1sc02347k>.
- 817 (46) Chakraborty, P.; Tang, Y.; Guterman, T.; Arnon, Z. A.; Yao, Y.; Wei, G.; Gazit, E. Co-
818 Assembly between Fmoc Diphenylalanine and Diphenylalanine within a 3D Fibrous
819 Viscous Network Confers Atypical Curvature and Branching. *Angew. Chemie - Int. Ed.*
820 **2020**, *59*, 23731–23739. <https://doi.org/10.1002/anie.202009488>.
- 821 (47) Fleming, S.; Debnath, S.; Frederix, P. W. J. M.; Hunt, N. T.; Ulijn, R. V. Insights into the
822 Coassembly of Hydrogelators and Surfactants Based on Aromatic Peptide Amphiphiles.
823 *Biomacromolecules* **2014**, *15*, 1171–1184. <https://doi.org/10.1021/bm401720z>.
- 824 (48) Diaferia, C.; Morelli, G.; Accardo, A. Fmoc-Diphenylalanine as a Suitable Building Block
825 for the Preparation of Hybrid Materials and Their Potential Applications. *J. Mater. Chem.*

- 826 *B* **2019**, 7, 5142–5155. <https://doi.org/10.1039/c9tb01043b>.
- 827 (49) Halperin-Sternfeld, M.; Ghosh, M.; Sevostianov, R.; Grigoriants, I.; Adler-Abramovich, L.
828 Molecular Co-Assembly as a Strategy for Synergistic Improvement of the Mechanical
829 Properties of Hydrogels. *Chem. Commun.* **2017**, 53, 9586–9589.
830 <https://doi.org/10.1039/c7cc04187j>.
- 831 (50) Nagy, K. J.; Giano, M. C.; Jin, A.; Pochan, D. J.; Schneider, J. P. Enhanced Mechanical
832 Rigidity of Hydrogels Formed from Enantiomeric Peptide Assemblies. *J. Am. Chem. Soc.*
833 **2011**, 133, 14975–14977. <https://doi.org/10.1021/ja206742m>.
- 834 (51) Swanekamp, R. J.; Welch, J. J.; Nilsson, B. L. Proteolytic Stability of Amphipathic
835 Peptide Hydrogels Composed of Self-Assembled Pleated β -Sheet or Coassembled Rippled
836 β -Sheet Fibrils. *Chem. Commun.* **2014**, 50, 10133–10136.
837 <https://doi.org/10.1039/c4cc04644g>.
- 838 (52) Cinar, G.; Ceylan, H.; Urel, M.; Erkal, T. S.; Deniz Tekin, E.; Tekinay, A. B.; Dâna, A.;
839 Guler, M. O. Amyloid Inspired Self-Assembled Peptide Nanofibers. *Biomacromolecules*
840 **2012**, 13, 3377–3387. <https://doi.org/10.1021/bm301141h>.
- 841 (53) Boothroyd, S.; Saiani, A.; Miller, A. F. Controlling Network Topology and Mechanical
842 Properties of Co-Assembling Peptide Hydrogels. *Biopolymers* **2014**, 101, 669–680.
843 <https://doi.org/10.1002/bip.22435>.
- 844 (54) Scelsi, A.; Bochicchio, B.; Smith, A.; Workman, V. L.; Castillo Diaz, L. A.; Saiani, A.;
845 Pepe, A. Tuning of Hydrogel Stiffness Using a Two-Component Peptide System for
846 Mammalian Cell Culture. *J. Biomed. Mater. Res. - Part A* **2019**, 107, 535–544.
847 <https://doi.org/10.1002/jbm.a.36568>.

- 848 (55) Abul-Haija, Y. M.; Scott, G. G.; Sahoo, J. K.; Tuttle, T.; Ulijn, R. V. Cooperative, Ion-
849 Sensitive Co-Assembly of Tripeptide Hydrogels. *Chem. Commun.* **2017**, *53*, 9562–9565.
850 <https://doi.org/10.1039/c7cc04796g>.
- 851 (56) Giraud, T.; Hoschtettler, P.; Pickaert, G.; Averlant-Petit, M. C.; Stefan, L. Emerging Low-
852 Molecular Weight Nucleopeptide-Based Hydrogels: State of the Art, Applications,
853 Challenges and Perspectives. *Nanoscale* **2022**, *14*, 4908–4921.
854 <https://doi.org/10.1039/d1nr06131c>.
- 855 (57) Peters, G. M.; Davis, J. T. Supramolecular Gels Made from Nucleobase, Nucleoside and
856 Nucleotide Analogs. *Chem. Soc. Rev.* **2016**, *45*, 3188–3206.
857 <https://doi.org/10.1039/c6cs00183a>.
- 858 (58) Pu, F.; Ren, J.; Qu, X. Nucleobases, Nucleosides, and Nucleotides: Versatile Biomolecules
859 for Generating Functional Nanomaterials. *Chem. Soc. Rev.* **2018**, *47*, 1285–1306.
860 <https://doi.org/10.1039/c7cs00673j>.
- 861 (59) del Prado, A.; González-Rodríguez, D.; Wu, Y. L. Functional Systems Derived from
862 Nucleobase Self-Assembly. *ChemistryOpen* **2020**, *9*, 409–430.
863 <https://doi.org/10.1002/open.201900363>.
- 864 (60) Li, X.; Kuang, Y.; Lin, H. C.; Gao, Y.; Shi, J.; Xu, B. Supramolecular Nanofibers and
865 Hydrogels of Nucleopeptides. *Angew. Chemie - Int. Ed.* **2011**, *50*, 9365–9369.
866 <https://doi.org/10.1002/anie.201103641>.
- 867 (61) Yuan, D.; Du, X.; Shi, J.; Zhou, N.; Zhou, J.; Xu, B. Mixing Biomimetic Heterodimers of
868 Nucleopeptides to Generate Biocompatible and Biostable Supramolecular Hydrogels.
869 *Angew. Chemie - Int. Ed.* **2015**, *54*, 5705–5708. <https://doi.org/10.1002/anie.201412448>.

- 870 (62) Baek, K.; Noblett, A. D.; Ren, P.; Suggs, L. J. Design and Characterization of
871 Nucleopeptides for Hydrogel Self-Assembly. *ACS Appl. Bio Mater.* **2019**, *2*, 2812–2821.
872 <https://doi.org/10.1021/acsabm.9b00229>.
- 873 (63) Giraud, T.; Bouguet-Bonnet, S.; Stébé, M. J.; Richaudeau, L.; Pickaert, G.; Averlant-Petit,
874 M. C.; Stefan, L. Co-Assembly and Multicomponent Hydrogel Formation upon Mixing
875 Nucleobase-Containing Peptides. *Nanoscale* **2021**, *13*, 10566–10578.
876 <https://doi.org/10.1039/d1nr02417e>.
- 877 (64) DiMaio, J. T. M.; Doran, T. M.; Ryan, D. M.; Raymond, D. M.; Nilsson, B. L. Modulating
878 Supramolecular Peptide Hydrogel Viscoelasticity Using Biomolecular Recognition.
879 *Biomacromolecules* **2017**, *18*, 3591–3599. <https://doi.org/10.1021/acs.biomac.7b00925>.
- 880 (65) Freeman, R.; Han, M.; Álvarez, Z.; Lewis, J. A.; Wester, J. R.; Stephanopoulos, N.;
881 McClendon, M. T.; Lynsky, C.; Godbe, J. M.; Sangji, H.; Luijten, E.; Stupp, S. I.
882 Reversible Self-Assembly of Superstructured Networks. *Science* **2018**, *362*, 808–813.
883 <https://doi.org/10.1126/science.aat6141>.
- 884 (66) Lee, W.; Tonelli, M.; Markley, J. L. NMRFAM-SPARKY: Enhanced Software for
885 Biomolecular NMR Spectroscopy. *Bioinformatics* **2015**, *31*, 1325–1327.
886 <https://doi.org/10.1093/bioinformatics/btu830>.
- 887 (67) Giraud, T.; Bouguet-Bonnet, S.; Marchal, P.; Pickaert, G.; Averlant-Petit, M. C.; Stefan, L.
888 Improving and Fine-Tuning the Properties of Peptide-Based Hydrogels: Via Incorporation
889 of Peptide Nucleic Acids. *Nanoscale* **2020**, *12*, 19905–19917.
890 <https://doi.org/10.1039/d0nr03483e>.
- 891 (68) Kong, J.; Yu, S. Fourier Transform Infrared Spectroscopic Analysis of Protein Secondary

- 892 Structures Protein FTIR Data Analysis and Band Assignment. *Acta Biochimica Biophysica*
893 *Sinica*, **2007**, *39*, 549–559.
- 894 (69) Banyay, M.; Sarkar, M.; Gräslund, A. A Library of IR Bands of Nucleic Acids in Solution.
895 *Biophys. Chem.* **2003**, *104*, 477–488. [https://doi.org/10.1016/S0301-4622\(03\)00035-8](https://doi.org/10.1016/S0301-4622(03)00035-8).
- 896 (70) Groenning, M. Binding Mode of Thioflavin T and Other Molecular Probes in the Context
897 of Amyloid Fibrils-Current Status. *J. Chem. Biol.* **2010**, *3*, 1–18.
898 <https://doi.org/10.1007/s12154-009-0027-5>.
- 899 (71) Nygren, J.; Svanvik, N.; Kubista, M. Interactions between the Fluorescent Dye Thiazole
900 Orange and DNA. *Biopolymers.* **1998**, *46*, 39–51. [https://doi.org/10.1002/\(sici\)1097-
901 0282\(199807\)46:1<39::aid-bip4>3.3.co;2-m](https://doi.org/10.1002/(sici)1097-0282(199807)46:1<39::aid-bip4>3.3.co;2-m).
- 902 (72) Arosio, P.; Knowles, T. P. J.; Linse, S. On the Lag Phase in Amyloid Fibril Formation.
903 *Phys. Chem. Chem. Phys.* **2015**, *17*, 7606–7618. <https://doi.org/10.1039/c4cp05563b>.
- 904 (73) Piotto, M.; Saudek, V.; Sklenář, V. Gradient-Tailored Excitation for Single-Quantum
905 NMR Spectroscopy of Aqueous Solutions. *J. Biomol. NMR* **1992**, *2*, 661–665.
906 <https://doi.org/10.1007/BF02192855>.
- 907 (74) Guilbaud, J. B.; Vey, E.; Boothroyd, S.; Smith, A. M.; Ulijn, R. V.; Saiani, A.; Miller, A.
908 F. Enzymatic Catalyzed Synthesis and Triggered Gelation of Ionic Peptides. *Langmuir*
909 **2010**, *26*, 11297–11303. <https://doi.org/10.1021/la100623y>.
- 910 (75) Mosseri, A.; Sancho-Alberero, M.; Leone, M.; Nava, D.; Secundo, F.; Maggioni, D.; De
911 Cola, L.; Romanelli, A. Chiral Fibers Formation Upon Assembly of Tetraphenylalanine
912 Peptide Conjugated to a PNA Dimer. *Chem. - A Eur. J.* **2022**, *28*, e202200693.
913 <https://doi.org/10.1002/chem.202200693>.

- 914 (76) Bonifazi, D.; Carloni, L. E.; Corvaglia, V.; Delforge, A. Peptide Nucleic Acids in
915 Materials Science. *Artif. DNA PNA XNA* **2012**, *3*, 112–122.
916 <https://doi.org/10.4161/adna.21941>.
- 917 (77) Quijano, E.; Bahal, R.; Ricciardi, A.; Saltzman, W. M.; Glazer, P. M. Therapeutic Peptide
918 Nucleic Acids: Principles, Limitations, and Opportunities. *Yale J. Biol. Med.* **2017**, *90*,
919 583–598.
- 920 (78) Bertolani, A.; Pirrie, L.; Stefan, L.; Houbenov, N.; Haataja, J. S.; Catalano, L.; Terraneo,
921 G.; Giancane, G.; Valli, L.; Milani, R.; Ikkala, O.; Resnati, G.; Metrangolo, P.
922 Supramolecular Amplification of Amyloid Self-Assembly by Iodination. *Nat. Commun.*
923 **2015**, *6*, 7574. <https://doi.org/10.1038/ncomms8574>.
- 924 (79) Hiew, S. H.; Mohanram, H.; Ning, L.; Guo, J.; Sánchez-Ferrer, A.; Shi, X.; Pervushin, K.;
925 Mu, Y.; Mezzenga, R.; Miserez, A. A Short Peptide Hydrogel with High Stiffness Induced
926 by 310-Helices to β -Sheet Transition in Water. *Adv. Sci.* **2019**, *6*, 1901173.
927 <https://doi.org/10.1002/advs.201901173>.
- 928 (80) Loo, Y.; Lakshmanan, A.; Ni, M.; Toh, L. L.; Wang, S.; Hauser, C. A. E. Peptide Bioink:
929 Self-Assembling Nanofibrous Scaffolds for Three-Dimensional Organotypic Cultures.
930 *Nano Lett.* **2015**, *15*, 6919–6925. <https://doi.org/10.1021/acs.nanolett.5b02859>.
- 931 (81) Maity, I.; Rasale, D. B.; Das, A. K. Sonication Induced Peptide-Appended Bolaamphiphile
932 Hydrogels for in Situ Generation and Catalytic Activity of Pt Nanoparticles. *Soft Matter*
933 **2012**, *8*, 5301–5308. <https://doi.org/10.1039/c2sm25126d>.
- 934 (82) Bettens, T.; Lacanau, V.; Van Lommel, R.; De Maeseneer, T.; Vandeplassche, W.;
935 Bertouille, J.; Brancart, J.; Barlow, T. M. A.; Woller, T.; Van Den Brande, N.;

- 936 Moldenaers, P.; De Proft, F.; Madder, A.; Hoogenboom, R.; Martin, C.; Ballet, S.; Alonso,
937 M. Towards the Understanding of Halogenation in Peptide Hydrogels: A Quantum
938 Chemical Approach. *Mater. Adv.* **2021**, *2*, 4792–4803.
939 <https://doi.org/10.1039/d1ma00455g>.
- 940 (83) Kleinsmann, A. J.; Nachtsheim, B. J. Phenylalanine-Containing Cyclic Dipeptides – the
941 Lowest Molecular Weight Hydrogelators Based on Unmodified Proteinogenic Amino
942 Acids. *Chem. Commun.* **2013**, *49*, 7818–7820. <https://doi.org/10.1039/c3cc44110e>.
- 943 (84) Zanna, N.; Tomasini, C. Peptide-Based Physical Gels Endowed with Thixotropic
944 Behaviour. *Gels* **2017**, *3*, 39. <https://doi.org/10.3390/gels3040039>.
- 945 (85) Baek, K.; Noblett, A. D.; Ren, P.; Suggs, L. J. Self-Assembled Nucleo-Triptide
946 Hydrogels Provide Local and Sustained Doxorubicin Release. *Biomater. Sci.* **2020**, *8*,
947 3130–3137. <https://doi.org/10.1039/d0bm00134a>.
- 948 (86) Zhai, Z.; Xu, K.; Mei, L.; Wu, C.; Liu, J.; Liu, Z.; Wan, L.; Zhong, W. Co-Assembled
949 Supramolecular Hydrogels of Cell Adhesive Peptide and Alginate for Rapid Hemostasis
950 and Efficacious Wound Healing. *Soft Matter* **2019**, *15*, 8603–8610.
951 <https://doi.org/10.1039/c9sm01296f>.
- 952 (87) Yan, C.; Pochan, D. J. Rheological Properties of Peptide-Based Hydrogels for Biomedical
953 and Other Applications. *Chem. Soc. Rev.* **2010**, *39*, 3528–3540.
954 <https://doi.org/10.1039/b919449p>.
- 955 (88) Denzer, B. R.; Kulchar, R. J.; Huang, R. B.; Patterson, J. Advanced Methods for the
956 Characterization of Supramolecular Hydrogels. *Gels* **2021**, *7*, 158.
957 <https://doi.org/10.3390/gels7040158>.

- 958 (89) Xue, C.; Lin, T. Y.; Chang, D.; Guo, Z. Thioflavin T as an Amyloid Dye: Fibril
959 Quantification, Optimal Concentration and Effect on Aggregation. *R. Soc. Open Sci.* **2017**,
960 *4*, 160696. <https://doi.org/10.1098/rsos.160696>.
- 961 (90) Amdursky, N.; Erez, Y.; Huppert, D. Molecular Rotors: What Lies behind the High
962 Sensitivity of the Thioflavin-T Fluorescent Marker. *Acc. Chem. Res.* **2012**, *45*, 1548–1557.
963 <https://doi.org/10.1021/ar300053p>.
- 964 (91) Haidekker, M. A.; Theodorakis, E. A. Environment-Sensitive Behavior of Fluorescent
965 Molecular Rotors. *J. Biol. Eng.* **2010**, *4*, 11. <https://doi.org/10.1186/1754-1611-4-11>.
- 966 (92) Wang, K.; Keasling, J. D.; Muller, S. J. Effects of the Sequence and Size of Non-Polar
967 Residues on Self-Assembly of Amphiphilic Peptides. *Int. J. Biol. Macromol.* **2005**, *36*,
968 232–240. <https://doi.org/10.1016/j.ijbiomac.2005.06.006>.
- 969 (93) Marchesan, S.; Easton, C. D.; Styan, K. E.; Waddington, L. J.; Kuskaki, F.; Goodall, L.;
970 McLean, K. M.; Forsythe, J. S.; Hartley, P. G. Chirality Effects at Each Amino Acid
971 Position on Tripeptide Self-Assembly into Hydrogel Biomaterials. *Nanoscale* **2014**, *6*,
972 5172–5180. <https://doi.org/10.1039/c3nr06752a>.
- 973 (94) Chen, L.; Morris, K.; Laybourn, A.; Elias, D.; Hicks, M. R.; Rodger, A.; Serpell, L.;
974 Adams, D. J. Self-Assembly Mechanism for a Naphthalene-Dipeptide Leading to
975 Hydrogelation. *Langmuir* **2010**, *26*, 5232–5242. <https://doi.org/10.1021/la903694a>.
- 976 (95) Meisl, G.; Kirkegaard, J. B.; Arosio, P.; Michaels, T. C. T.; Vendruscolo, M.; Dobson, C.
977 M.; Linse, S.; Knowles, T. P. J. Molecular Mechanisms of Protein Aggregation from
978 Global Fitting of Kinetic Models. *Nat. Protoc.* **2016**, *11*, 252–272.
979 <https://doi.org/10.1038/nprot.2016.010>.

- 980 (96) Braun, G. A.; Dear, A. J.; Sanagavarapu, K.; Zetterberg, H.; Linse, S. Amyloid- β Peptide
981 37, 38 and 40 Individually and Cooperatively Inhibit Amyloid- β 42 Aggregation. *Chem.*
982 *Sci.* **2022**, *13*, 2423–2439. <https://doi.org/10.1039/d1sc02990h>.
- 983 (97) Knowles, T. P. J.; Waudby, C. A.; Devlin, G. L.; Cohen, S. I. A.; Aguzzi, A.; Vendruscolo,
984 M.; Terentjev, E. M.; Welland, M. E.; Dobson, C. M. An Analytical Solution to the
985 Kinetics of Breakable Filament Assembly. *Science*. **2009**, *326*, 1533–1537.
986 <https://doi.org/10.1126/science.1178250>.
- 987 (98) Cukalevski, R.; Yang, X.; Meisl, G.; Weininger, U.; Bernfur, K.; Frohm, B.; Knowles, T.
988 P. J.; Linse, S. The A β 40 and A β 42 Peptides Self-Assemble into Separate Homomolecular
989 Fibrils in Binary Mixtures but Cross-React during Primary Nucleation. *Chem. Sci.* **2015**, *6*,
990 4215–4233. <https://doi.org/10.1039/c4sc02517b>.
- 991 (99) Barton, J.; Sebastian Arias, D.; Niyangoda, C.; Borjas, G.; Le, N.; Mohamed, S.; Muschol,
992 M. Kinetic Transition in Amyloid Assembly as a Screening Assay for Oligomer-Selective
993 Dyes. *Biomolecules* **2019**, *9*, 539. <https://doi.org/10.3390/biom9100539>.
- 994 (100) Hasecke, F.; Miti, T.; Perez, C.; Barton, J.; Schölzel, D.; Gremer, L.; Grüning, C. S. R.;
995 Matthews, G.; Meisl, G.; Knowles, T. P. J.; Willbold, D.; Neudecker, P.; Heise, H.; Ullah,
996 G.; Hoyer, W.; Muschol, M. Origin of Metastable Oligomers and Their Effects on
997 Amyloid Fibril Self-Assembly. *Chem. Sci.* **2018**, *9*, 5937–5948.
998 <https://doi.org/10.1039/C8SC01479E>.
- 999 (101) Draper, E. R.; Adams, D. J. How Should Multicomponent Supramolecular Gels Be
1000 Characterised? *Chem. Soc. Rev.* **2018**, *47*, 3395–3405. <https://doi.org/10.1039/c7cs00804j>.
- 1001 (102) Suss, O.; Motiei, L.; Margulies, D. Broad Applications of Thiazole Orange in Fluorescent

- 1002 Sensing of Biomolecules and Ions. *Molecules* **2021**, *26*, 2828.
1003 <https://doi.org/10.3390/molecules26092828>.
- 1004 (103) Sarroukh, R.; Goormaghtigh, E.; Ruyschaert, J. M.; Raussens, V. ATR-FTIR: A
1005 “Rejuvenated” Tool to Investigate Amyloid Proteins. *Biochim. Biophys. Acta - Biomembr.*
1006 **2013**, *1828*, 2328–2338. <https://doi.org/10.1016/j.bbamem.2013.04.012>.
- 1007 (104) Kelly, S. M.; Jess, T. J.; Price, N. C. How to Study Proteins by Circular Dichroism.
1008 *Biochimica et Biophysica Acta - Proteins and Proteomics.* **2005**, *1751*, 119–139.
1009 <https://doi.org/10.1016/j.bbapap.2005.06.005>.
- 1010 (105) Corradini, R.; Tedeschi, T.; Sforza, S.; Marchelli, R. Electronic Circular Dichroism of
1011 Peptide Nucleic Acids and Their Analogues. In *Comprehensive Chiroptical Spectroscopy*;
1012 2012; Vol. 2, pp 587–614. <https://doi.org/10.1002/9781118120392.ch18>.
- 1013 (106) Koch, T.; Naesby, M.; Wittung, P.; Jørgensen, M.; Larsson, C.; Buchardt, O.; Stanley, C.
1014 J.; Nordén, B.; Nielsen, P. E.; Ørum, H. PNA-Peptide Chimeras. *Tetrahedron Lett.* **1995**,
1015 *36*, 6933. [https://doi.org/10.1016/00404-0399\(50\)1373P-](https://doi.org/10.1016/00404-0399(50)1373P-).
- 1016 (107) Diaferia, C.; Roviello, V.; Morelli, G.; Accardo, A. Self-Assembly of PEGylated
1017 Diphenylalanines into Photoluminescent Fibrillary Aggregates. *ChemPhysChem* **2019**, *20*,
1018 2774–2782. <https://doi.org/10.1002/cphc.201900884>.
- 1019 (108) Ziaunys, M.; Smirnovas, V. Emergence of Visible Light Optical Properties of L-
1020 Phenylalanine Aggregates. *PeerJ* **2019**, *7*, e6518. <https://doi.org/10.7717/peerj.6518>.
- 1021 (109) Brown, R. F.; Andrews, C. T.; Elcock, A. H. Stacking Free Energies of All DNA and RNA
1022 Nucleoside Pairs and Dinucleoside-Monophosphates Computed Using Recently Revised
1023 AMBER Parameters and Compared with Experiment. *J. Chem. Theory Comput.* **2015**, *11*,

- 1024 2315–2328. <https://doi.org/10.1021/ct501170h>.
- 1025 (110) Wolfram Saenger. *Principles of Nucleic Acid Structure*, 1st ed.; Springer New York, N.,
1026 Ed.; **1984**. <https://doi.org/10.1007/978-1-4612-5190-3>.
- 1027 (111) Avitabile, C.; Diaferia, C.; Roviello, V.; Altamura, D.; Giannini, C.; Vitagliano, L.;
1028 Accardo, A.; Romanelli, A. Fluorescence and Morphology of Self-Assembled Nucleobases
1029 and Their Diphenylalanine Hybrid Aggregates. *Chem. - A Eur. J.* **2019**, *25*, 14850–14857.
1030 <https://doi.org/10.1002/chem.201902709>.
- 1031 (112) Demchenko, A. P. The Red-Edge Effects: 30 Years of Exploration. *Luminescence* **2002**,
1032 *17*, 19-42. <https://doi.org/10.1002/bio.671>.
- 1033 (113) Berger, O.; Adler-Abramovich, L.; Levy-Sakin, M.; Grunwald, A.; Liebes-Peer, Y.;
1034 Bachar, M.; Buzhansky, L.; Mossou, E.; Forsyth, V. T.; Schwartz, T.; Ebenstein, Y.;
1035 Frolow, F.; Shimon, L. J. W.; Patolsky, F.; Gazit, E. Light-Emitting Self-Assembled
1036 Peptide Nucleic Acids Exhibit Both Stacking Interactions and Watson-Crick Base Pairing.
1037 *Nat. Nanotechnol.* **2015**, *10*, 353–360. <https://doi.org/10.1038/nnano.2015.27>.
- 1038 (114) Yu, Y.; Gim, S.; Kim, D.; Arnon, Z. A.; Gazit, E.; Seeberger, P. H.; Delbianco, M.
1039 Oligosaccharides Self-Assemble and Show Intrinsic Optical Properties. *J. Am. Chem. Soc.*
1040 **2019**, *141*, 4833–4838. <https://doi.org/10.1021/jacs.8b11882>.
- 1041 (115) Haldar, S.; Chaudhuri, A.; Chattopadhyay, A. Organization and Dynamics of Membrane
1042 Probes and Proteins Utilizing the Red Edge Excitation Shift. *J. Phys. Chem. B* **2011**, *115*,
1043 5693–5706. <https://doi.org/10.1021/jp200255e>.
- 1044 (116) Han, X.; Leroy, J. L.; Guéron, M. An Intramolecular I-Motif: The Solution Structure and
1045 Base-Pair Opening Kinetics of d(5mCCT3CCT3ACCT3CC). *J. Mol. Biol.* **1998**, *278*,

- 1046 949–965. <https://doi.org/10.1006/jmbi.1998.1740>.
- 1047 (117) Shapiro, Y. E. Structure and Dynamics of Hydrogels and Organogels: An NMR
1048 Spectroscopy Approach. *Prog. Polym. Sci.* **2011**, *36*, 1184–1253.
1049 <https://doi.org/10.1016/j.progpolymsci.2011.04.002>.
- 1050 (118) Atkinson, R. A. NMR of Proteins and Nucleic Acids. In *Nuclear Magnetic Resonance*;
1051 The Royal Society of Chemistry, **2021**; Vol. 46, pp 250–271.
1052 <https://doi.org/10.1039/9781788010665-00250>.
- 1053